Sensitivity analysis of fusion power plant designs using the SYCOMORE system code

S. Kahn, C. Reux, J.-F Artaud, G Aiello, J.-B Blanchard, J. Bucalossi, S Dardour, L Di Gallo, D Galassi, Frédéric Imbeaux, et al.

Sensitivity analysis of fusion power plant designs using the SYCOMORE system code

S. Kahn[1], C. Reux[1], J.-F. Artaud[1], G. Aiello[2], J.-B. Blanchard[3], J. Bucalossi[1], S. Dardour[4], L. Di Gallo[1], D. Galassi[5], F. Imbeaux[1], J.-C. Jaboulay[2], M. Owsiak[6], N. Piot[1], R. Radhakrishnan[1], L. Zani[1] and the URANIE team

1 CEA, IRFM F-13108 Saint-Paul-Lez-Durance, France
2 CEA-Saclay, DEN, DM2S, SERMA, F-91191 Gif-sur-Yvette, France
3 CEA-Saclay, DEN, STMF, F-91191 Gif-sur-Yvette
4 IAEA, Vienna International Centre, PO Box 100, 1400 Vienna, Austria
5 Aix Marseille Univ, CNRS, Centrale Marseille, M2P2 Marseille, France
6 Poznan Supercomputing and Networking Center; IChb PAS, Noskowskiego 12/14,61-704 Poznan, Poland

E-mail: `sebastien.kahn@cea.fr`

Febuary 2019

Abstract. The next step after ITER is the demonstration of stable electricity production with a fusion reactor. Key design performances will have to be met by the corresponding power plant demonstrator (DEMO), fulfilling a large number of constraints. System codes such as SYCOMORE, by simulating all the fusion power plant sub-systems, address those questions. To be able to perform design optimizations, simplified models relying on physical and technological assumptions have to be used, resulting in a large number of input parameters. As these parameters are not always exactly known, the impact of their associated uncertainties on final design performances has to be evaluated. Sensitivity methods, by measuring the relative influence of inputs on the figures of merit of the design, allow to select the dominant parameters. This information helps the search for optimal working points, guides the priority for technical improvements and finally allows selecting meaningful inputs for uncertainty propagation. A full set of sensitivity methods and their application on a ITER and a DEMO design will be presented, discussing both the statistical methods behaviors and the physical results. Plasma shape parameters (minor radius and plasma elongations) share half of the net electricity power sensitivity for the DEMO 2015 design while the toroidal magnetic field and the 95 % safety factor are responsible for 23% and 17% of the electric power sensitivity, respectively. The plasma minor radius is responsible for 45% of the pulse duration sensitivity for the DEMO 2015 design, while plasma physics parameters drive $\sim 37\%$ of the pulse duration sensitivity.

1. Introduction

The next step after ITER would be a demonstration power plant (DEMO), producing sustainable electricity power. For this purpose, a stable high performance plasma is necessary. To accommodate such extreme condition with the numerous fusion power plant constraints (plasma facing components protection, superconducting coil protection, tritium recycling etc ...) in a consistent way, dedicated system codes, aiming to simulate all power plant sub-systems with their interactions, are necessary.

The SYCOMORE system code [1], developed at the CEA/IRFM organization, is a set of independent simplified models (modules) communicating through the Integrated Modeling Framework (ITM) data structures. For each module and each loop between modules, the consistency of the design is checked, making sure that only viable designs are retained. The core physics is simulated using the Helios code [2], using the plasma profiles as an input to compute the steady-state power balance. The Scrape-Off Layer (SOL) is modelled using an advanced two points model [3], taking into account momentum losses and impurity radiation.

As impurity radiation affects both the core and the SOL power balance, a loop between the two corresponding modules is designed to find the minimal impurity fractions ($f_{Imp} \equiv \frac{n_{Imp}}{n_e}$) necessary to protect the divertor targets from both intolerable heat flux per unit of surface (q_{peak}) and tungsten sputtering (maximum target plasma temperature $T_{targets}$). This loop, described in appendix Appendix A, also ensure consistent boundary conditions between the SOL and the core plasma. A surrogate model trained on advanced neutronics calculations [4, 5] computes the thickness of the tritium breeding blankets (based on the Helium Cooled Lithium Lead - HCLL technology) necessary to achieve the required Tritium Breeding Ratio (TBR - number of tritium atoms produced per fusion neutron). It also calculates the shield thickness needed to protect the inner leg of the Toroidal Field Coil from excessive neutron flux. The Toroidal Field coil (TF) is modelled [6] and the TF width necessary to generate the prescribed magnetic field on plasma axis is deduced. The Central Solenoid (CS) magnet is sized to fit in the remaining space in the centre of the tokamak and is modelled [6] to calculate the generated flux, allowing to estimate the pulse duration [2]. Stresses calculations are performed for both CS and TF magnets to estimate the quantity of steel necessary to hold the stresses generated by the Lorentz forces, providing a coherent radial build for the two magnets. A power conversion module computes the efficiency of the various thermodynamical cycles generating electricity from primary heat [7]. A module then calculates the fraction of tritium burnt in the plasma by the fusion reaction [8]. The global power balance of the reactor is finally computed to estimate the net electricity power production.

As simplified models are used in SYCOMORE, numerous assumptions are necessary to define a design. They result in the choice of different scaling laws or model parametrization and can have a great impact on the final power plant design. Reflecting the current knowledge on the physical and engineering constrains, these input parameters are not always precisely known. To provide robust designs, those uncertainties must be propagated to the different figures of merit (outputs) used in the design optimization, such as net electricity power production or plasma pulse duration for DEMO. This question can be simply addressed using a Monte-Carlo uncertainty propagation, as it has been done with the PROCESS system code [9, 10, 11]. Such a method, also implemented in SYCOMORE, uses a brute-force exploration of the input phase-space. A large number of power plant designs must thus be evaluated to obtain robust results with respect to statistical uncertainty, reflecting the quality of the input phase-space exploration. As the required number of design evaluations rapidly grow with the dimension of the input phase, only a reduced number of uncertainties sources should be propagated by this method. More general sensitivity analyses are therefore necessary to select the dominant uncertainty sources for the Monte-Carlo uncertainty propagation.

Dedicated algorithms, implemented in the SYCOMORE code will be presented in section 2. A sensitivity analysis evaluating the relative impact of 6 parameters on the ITER design will be presented starting from the ITER design [12, 13]. Finally, a more general sensitivity analysis (48 inputs) is performed starting from the DEMO 2015 pulsed design [14] and compared to the initial analysis presented in Ref. [14]. The definition of the variables used in this document are percised in Appendix B.

2. SYCOMORE sensitivity algorithms

2.1. Aim of a sensitivity analysis

In the case of non-linear models, the number of runs necessary for uncertainty propagation or metamodel definition has an exponential dependency on the number of inputs (an additional input adds a dimension for the analysis). SYCOMORE, with more than a hundred inputs and several non-linear models, is not suited for raw uncertainty propagations as it would require a prohibitive number of runs. Sensitivity analyses [15, 16], providing a ranking of each input uncer-

tainty contribution to the output ones, help selecting the dominant inputs to perform uncertainty propagations with a smaller input dimension. Such ranking depends on both the range/shape of the input distributions (assumptions on the inputs uncertainties) and the model itself (the SYCOMORE code). An interesting by-product of some sensitivity analysis methods is the evaluation of the linearity and/or the additivity of the models in the considered range.

A model of the output Y is considered additive when it can be written as

$$Y = \beta_0 + \sum_i f_i(X_i)$$

with β_0 a real number, X_i the model inputs labelled by the index i and f_i an arbitrary function depending only on X_i. If the model contains non-additive terms, such as X_iX_j, the influence of X_i on Y depends on the value of X_j. This effect is defined in this paper as input interaction, to make a clear distinction with correlations brought by input distributions only. In the SYCOMORE such interactions can typically arise from power laws used to approximate the energy confinement time or the pedestal electron temperature. As the sensitivity ranks values, the intensity of input interaction depends on the input distribution ranges and shapes.

Linear models are a sub-set of the additive models defined as

$$Y = \beta_0 + \sum_{i=1}^{n_X} \beta_i X_i$$

with β_i being a real number (linear coefficients) associated to the input X_i.

Two different class of methods are considered, following the Occam razor principle:

- **linearization methods**. If the model is linear, the sensitivity coefficient SRC_i can be simply deduced from their linear coefficients term β_i:

  $$SRC_i = \beta_i \frac{\sigma_{X_i}}{\sigma_Y}$$

  with σ_{X_i} and σ_Y the root mean square (RMS) associated to the input X_i and the output Y, respectively [15, 16]. Therefore, if the output can be fitted with a linear model, the sensitivity ranking is straightforward.
- **Global methods**. If the output shows non-linear dependencies within the input range, linearization methods are not valid anymore. Global methods, preserving the model structure, become then necessary. Two types of global methods can be distinguished.
  - *Screening methods*: the output difference associated to the variation of one parameter is estimated on different locations of the input phase-space. This kind of methods needs a small number of runs, but no estimation of the robustness of the results is possible.
  - *Variance methods*: based on variance decomposition, these methods indicates the fraction of variance due to each input or group of inputs. This allows to define both input sensitivity rankings and input interactions in a consistent way, but large number of runs is necessary.

Generally, screening methods are used to select a set of dominant variables to be analysed using variance methods, or regression methods if models are simple enough.

2.2. Sensitivity methods implemented in SYCOMORE

The implementation of the sensitivity algorithms is provided by the URANIE statistical framework [17] developed by the CEA. Three sensitivity methods have been selected: the linear/monotonic regression method [18], the Morris method [19] and a pick-and-freeze method for Sobol indexes estimation [20, 21].

2.2.1. Linear regression method

The linear regression method provides a sensitivity ranking assuming the output has a linear dependency with the inputs. The validity of the linear assumption is tested and statistical uncertainty associated to the ranking coefficient is estimated with indicative, even though not rigorous, 95% confidence levels. More precisely, a set of n_s SYCOMORE runs is executed varying n_X input parameters using a Latin Hypercube Sampling (LHS) [22] and a matrix $A(n_S, n_X + 1)$ is built. The linear coefficients $\beta = (\beta_0 \dots \beta_{n_X})$ are deduced from the output values $y = (y_0 \dots y_{n_S})$ using

$$\beta = (A^T A)^{-1} A^T y$$

The Standard Regression Coefficients SRC_i used in the sensitivity ranking, are then defined as

$$SRC_i = \beta_i \sqrt{\frac{Var(X_i)}{Var(Y)}}.$$

The outputs are then re-computed using the fitted linear model $\hat{y}_i$ to assert the quality of the regression:

$$R^2_{adj} = 1 - \left|1 - R^2\right| \left|\frac{n_S - 1}{n_S - (1 + n_X)}\right|$$

with

$$R^2 = 1 - \frac{\sum_{i=1}^{n_S}(y_i - \hat{y}_i)^2}{\sum_{i=1}^{n_S}(y_i - \bar{y}_i)^2}$$

$\bar{y}_i$ being the expectation of the sample using the fitted linear model. The linear regression is invalid if R_{adj} is low. Another way to verify the linear assumption is to compute the quadratic sum of the SRC coefficients, equal to 1 in case of a linear model. As the input phase-space is randomly sampled, some aspects of the model behaviour can be missed if the number of runs is not large enough to explore the input phase-space. To provide an estimate of this statistical effect, indicative 95% confidence level are computed using a Fisher Z-transform [23].

2.2.2. Monotonic regression method

Ranks can be built with the outputs associating 1 to the lowest output value and n_S to the largest one. Fitting these ranks with a linear regression allow computing the Standard Ranks Regression Coefficients $SRRC_i$, their associated R_{adj} and 95% confidence levels. Although the theoretical validity of the $SRRC_i$ has not been demonstrated, these coefficients provide indicative sensitivity ranks based on weaker assumptions that the SRC_i ones, suitable for more complex models.

2.2.3. Morris method

The Morris method [19] is a screening method, providing approximate ranks with a small number of runs and no model assumptions. This method is generally used to identify negligible variables to be removed from more complete sensitivity analysis (Regression or Sobol method). Once the dominant variables are selected, quantitative sensitivity rankings can be provided with associated statistical uncertainties (confidence levels). The principle of the Morris method is to compute the output difference varying only one input. This procedure is repeated r times for each input in different input phase-space regions, capturing the effect of potential non-linearity. Technically, a homogeneous input grid of p intervals is built and r trajectories (replicas) of n_X variations are defined with a random starting point as illustrated in figure 1. Each point of the trajectories is defined iteratively, randomly selecting the next variable to be varied and its variation direction. Once the outputs are computed for all the trajectory points, elementary effects EE_i^t are computed between two neighbouring points:

$$EE_i^t = \frac{y(X_i + \Delta_i) - y(X_i)}{\Delta_i}$$

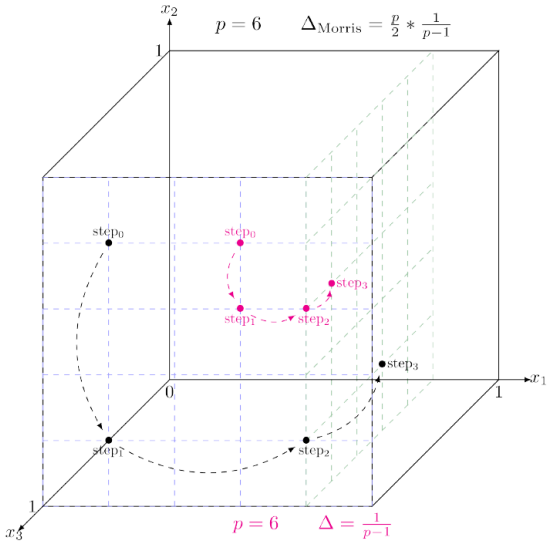

Figure 1: Schematic view of two trajectories drawn randomly in the discretized hyper-volume (with a grid containing 6 points) for two different values of the elementary variation Δ.

with i labelling the input X_i varied in a Δ_i interval (all other inputs remaining the same) and t labelling the random trajectory. Their mean absolute values over all trajectories $\langle |EE_i| \rangle = \frac{1}{r}\sum_{t=0}^{t=r} |EE_i^t|$ allow to identify inputs with negligible effects on the outputs and their standard deviation $\sigma(EE_i)$ provides a crude estimation of their linearity as $\sigma(EE_i) = 0$ for a linear model.

2.2.4. Sobol method

Sensitivity indexes [20] can be computed using the notion of conditional variance $Var(Y|X_i = x_i))$: the output Y variance obtained fixing one or a group of inputs X_i to a given value x_i. The more a variable is important, the smaller the expected value of the conditional variance $E(Var(Y|X_i))$ is compared to the total variance $Var(Y)$. Therefore, the ratio between those two quantities provide a well-defined sensitivity indicator. Normalized sensitivity indexes (Sobol indexes) are defined as $S_i = 1 - \frac{E(Var(Y|X_i))}{Var(Y)}$ and become, using the total variance theorem $Var(Y) = E(Var(Y|X_i)) + Var(E(Y|X_i))$:

$$S_i = \frac{Var(E(Y|X_i))}{Var(Y)}$$

Two kind of Sobol indexes are generally usually used:

- *First order indexes* (S_{first}): Sobol index associated to only one input. Besides providing a sensitivity ranking without model assumptions, these indexes provide useful additional information on

the model structure as their sum should be equal to one when the model is additive for instance. Moreover, in the case of a pure linear model they are equivalent to the linear regression coefficients, as $S_{first,i} = SRC_i^2$.

- *Total indexes* (S_{total}): sum of the all the Sobol indexes defined with input variables groups containing at least the input associated to the total index. If the considered input has no interaction with others in the model, first and total order indexes are equivalent. Their difference brings therefore an estimation of the interaction of each input with all others, providing precious information about the model.

In SYCOMORE, the Sobol indexes are computed using covariance matrices with a pick-and-freeze method based on a covariance matrix estimation [21], that provides an indicative 95% confidence level interval. Such method requires a large number of runs and should be used on a relatively small set of inputs.

2.3. Limitation of the SYCOMORE sensitivity methods

The Morris and the Sobol methods are incompatible with correlated inputs. Linear regression can nevertheless be used on this situation and an alternative of the Sobol indexes (Shapley indexes) can be used for non-linear models [24].

The algorithms used to evaluate the Morris and the Sobol indexes fail if any points are removed from their initial samplings. As keeping invalid designs can strongly bias the sensitivity results, these two methods must be used in a range where all designs are valid. A dedicated set of data visualization tools has been set up in SYCOMORE to help the user finding such phase-space. The produced graphics show both the invalid designs location and their causes (for example pellets plasma fuelling impossible or to small radial space available for the toroidal field coils etc..). A better formulation of the model can also significantly reduce the number of un-valid designs. For example, prior to the development of sensitivity analysis in SYCOMORE, the plasma density averaged electron temperature $< T_e >_n$ was used as a user input to parametrize the temperature profile. This led to a large number of invalid design in which the heating power was larger that the power losses. This issue has been solved by adding a loop on $< T_e >_n$ to determine its minimal value for a given auxiliary heating power, enforcing the steady-state power balance.

The real impact of several SYCOMORE inputs cannot be captured by the current methods. For example, the plasma major radius (R_{maj}) has a weak direct impact on plasma performances. But it defines the validity range of the plasma minor radius (a_{min}). As a_{min} has a strong influence on plasma performances, R_{maj} has a strong indirect impact on performances, which is not captured by the SYCOMORE sensitivity. More generally, threshold effects are not captured by sensitivity methods. Dedicated algorithms can nevertheless be used to quantify threshold/failure effects [25].

3. ITER study

The first sensitivity analysis focuses on key ITER design parameters (inputs) known with large uncertainties. These parameters are generally driven by diverse kind of considerations and it is difficult to propose an input probability distribution without a complex study of all the phenomena they reflect. For example, the energy confinement time enhancement factor (f_H) parametrises the scaling law fit uncertainty on current tokamaks data, but also physics extrapolation to larger scales and the ITER session leader choice on plasma scenario. As such study has not yet been performed, no prior knowledge has been assumed for the input distribution (flat shape). The selected inputs for this study are:

- **Toroidal magnetic field on axis (B_T) :**
  Technical issues such as defective seals or mechanical fatigue can lead to operate the toroidal field coils (TF) below their nominal performances at $B_T = 5.3$ T for safety reasons. To reflect this eventuality, B_T is varied from 4.0 T (degraded) to 5.3 T (baseline) [12].
- **Energy confinement enhancement (f_H) :**
  based on JET experiment, a 20% uncertainty on confinement time is set ($0.8< f_H <1.2$) [26]. Quantitative effects due to the much larger ITER dimension are impossible to predict with current codes, and thus not included in this uncertainty.
- **Separatrix density parameter ($f_{n_{sep}}$) :**
  defined as $f_{n_{sep}} = \frac{n_e(sep)}{f_{GW} n_{GW}}$, with f_{GW} and n_{GW} the Greenwald fraction and density respectively, is a key parameter of the SOL two points model. $f_{n_{sep}}$ is varied from 0.3, usually observed in current tokamaks [26] to a much larger value: 0.9, potentially necessary to protect the ITER divertor [27].
- **Heating power (P_{add}) :**
  This input defines the necessary heating power to add to the α one, to obtain the steady-state power balance. SYCOMORE does not indicate the necessary power to achieve DT fusion ignition as time dependent simulation of the plasma current and the heating ramp-up must be performed for this purpose (this can be estimated with codes like METIS [28]). The ITER plasma heating will be sheared between neutral beam injection (NBI) providing $P_{NBI} =$ 33 MW and ECRH/ICRH antennas providing 20 MW each, leading to a nominal heating power of $P_{Heat} = 73$ MW [13]. Potential degradation of the antenna performances is considered by varying P_{Heat} between 33 MW (NBI only) and 73 MW (full heating capabilities).
- **scrape-off layer width (λ_q) :**
  This quantity, defined within larges uncertainties, is varied from the value predicted by the Eich scaling : $\lambda_q \approx 1$ mm [29], to the very optimistic value initially taken for the ITER design : $\lambda_q = 20$ mm [30].
- **SOL private region spreading factor (S_q) :**
  this quantity, defined in [31], reflects the divertor energy deposit spreading toward the SOL private region. The two points model describes only the parallel transport while the spreading factor is related to cross-field transport. Therefore this effect is only considered *a posteriori* on the divertor energy density constrain without affecting the electron temperature at the divertor targets. As large uncertainties are observed on the experimental scaling [29], S_q is conservatively varied between 1 and 15 mm.

As the IPB98(y,2) confinement time scaling law [32, p2202-2209] is used, H mode is assumed in this study. The variable $f_{L-H} = \frac{P_{sep}}{P_{L-H}^{Martin}}$, with P_{sep} the convected power crossing the separatrix and P_{L-H}^{Martin} the H-mode threshold predicted by the Martin scaling [33], addresses this assumption. As P_{L-H}^{Martin} is defined with large uncertainties, no sharp cut on this variable is applied, replaced by a dedicated sensitivity analysis. In parallel, a sensitivity analysis on fusion power P_{fus} [2] will be shown to address the uncertainties on plasma performance. After the ITER working point briefly presented (section 3.1, a sampling will be first used to visualize the f_{L-H} and P_{fus} inputs dependency in (section 3.2.1), then a linear regression method will be used to provide a first sensitivity ranking (section 3.2.2), complemented by the results of a Sobol method (section 3.2.3).

3.1. The ITER working point

The ITER working point is summarized in table 1. Argon impurity is used for divertor protection (beryllium and tungsten impurities from first walls and divertor are neglected). A small electron density profile peaking is assumed $\frac{n_e(0)}{n_e(ped)} = 1.023$, allowing large separatrix electron density values for efficient divertor protection. The upstream SOL width is set at $\lambda_q = 5$ mm corresponding to the values proposed in the reference [34] and the argon screening set at $\eta_{Ar} = \frac{f_{Ar}^{SOL}}{f_{Ar}^{core}} = 6$ close to the value usually assumed in other system codes such as PROCESS [9, 10]. The separatrix density parameter has been set to achieve a full H-mode following the Martin criteria: $f_{L-H} =1.5$ with $f_{n_{sep}} = 0.7$. A good agreement with the ITER baseline DT scenario is found with $P_{fus} = 502$ MW,

Input definitions	**Names**	**ITER**
Major/minor plasma radius	R_{maj}/a_{min}	6.2/2 m
Toroidal magnetic field on plasma axis	B_T	5.3 T
Safety factor at 95% flux surface	q_{95}	3
Upper/lower separatrix elongation	κ^{up}/κ^{low}	1.687/2.001
Upper/lower separatrix triangularity	δ^{up}/σ^{low}	0.466/0.568
Greenwald electron density fraction	f_{GW}	0.85
IPB98(y,2) confinement enhancement factor	f_H	1.00
Additional heating power	P_{add}	50.0 MW
Heat flux on divertor targets	q^{div}_{peak}	<10 MW·m^{-2}
Plasma electron temperature on divertor	T_e^{div}	<5 eV
Argon screening	$\eta_{Ar} = \frac{f_{Ar}^{SOL}}{f_{Ar}^{CORE}}$	6.0
Upstream Scrape-off layer (SOL) width	λ_q/S_q	5.0/1.5 mm
Central/pedestal/separatrix density	$n_e^{0/ped/sep}$	0.99/0.97/0.68 10^{20}m^{-3}
Central/pedestal/separatrix temperature	$T_e^{0/ped/sep}$	25/2.8/0.18 keV
Helium/argon fraction	f_{He}/f_{Ar}	3.28/0.027 %

Table 1: Main Inputs parameters used to define the ITER working point. The parameters in the three last rows are computed by the SYCOMORE system code.

a fusion gain of $Q = 9.9$ [13] and separatrix densities close to the ones used in SOLPS-ITER codes [27].

3.2. Results

3.2.1. Data visualization

Before using any sensitivity algorithms, it is interesting to visualize the figures of merit dependency with the inputs. A LHS [22] sampling (semi-random sampling providing a better repartition than a simple random sampling) of 5000 design points has been used to explore the inputs phase-space within the ranges presented in section 3. The output values has been separately projected onto each input X_{proj} to produce 1D plots. As all inputs are varied simultaneously, different outputs values can be obtained for a given X_{proj} value. The corresponding graphics will no longer be a simple line, but will have a width characterized by the corresponding conditional variance $Var(Y|X_{proj} = x_{proj})$. If $Var(Y|X_{proj} = x_{proj}) << Var(Y)$, X_{proj} is dominant in the x_{proj} neighborhood. It is interesting to observe that the mean value of these conditional variance directly defines the Sobol indexes (see section 2.2.4). Projections on more than one variable can also provide a better understanding of input interactions in the model. Figure 2 shows the f_{L-H} (sub-figure 2a) and P_{fus} (sub-figure 2b) projection over λ_q. Lateral left f_{L-H} and P_{fus} projection histograms has been added helping the visual estimation of $Var(Y)$ and the bottom histograms shows the λ_q sampling and the repartition of the failed runs if any. To help the visualization of the λ_q output dependency, the f_{L-H}/P_{fus} mean value (dark green horizontal bars) computed on homogeneous λ_q and its associated uncertainty (vertical dark green bars) is added.

Two regimes can be identified :

- low λ_q : Large λ_q dependency and small λ_q conditional variance (especially for f_{L-H}) indicating that λ_q is one of the dominant variables.
- high λ_q : reduced λ_q dependency with a larger conditional variance indicating larger contribution from other inputs.

λ_q only drives the quantity of argon used to protect the divertor targets, and hence influence the core through line radiation and D-T fuel dilution. Figure 3a shows the core argon fraction (f_{Ar}^{core}) projected on λ_q. f_{Ar}^{core} decreases with λ_q with a much larger slope at low λ_q than at high λ_q. This dependency is similar to the ones observed on f_{L-H} and P_{fus}, confirming that f_{Ar}^{core} is a good candidate to explain the two regimes. Figures 3b and 3c show the power dissipated through argon line radiation (P_{line}) in the core plasma and the energy confinement time (τ_E) projections on λ_q, respectively. On one hand, P_{line} decreases with λ_q with a much larger slope at low λ_q. On the other hand τ_E strongly decreases with λ_q at low λ_q whereas almost no dependency is observed at large λ_q (This behavior is expected as $\tau_E \propto < T_e >_n^{-2.2}$ [2], $< T_e >_n$ being the density average electron temperature of the plasma). The convected power through the separatrix (P_{sep}) naturally decrease at lower λ_q while P_{line} increases. At $\lambda_q = 2$ mm, the average P_{line} value ($\sim$ 40 MW) gets larger than

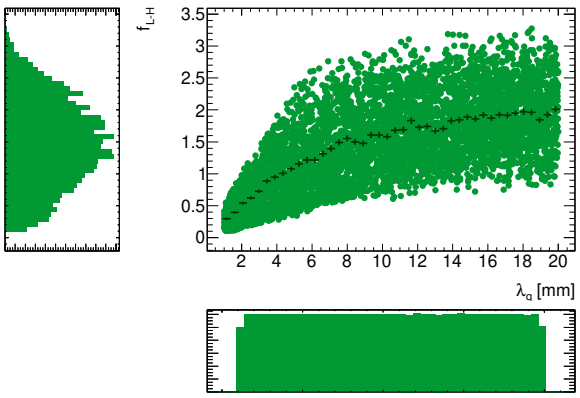

(a) f_{L-H} projected on λ_q

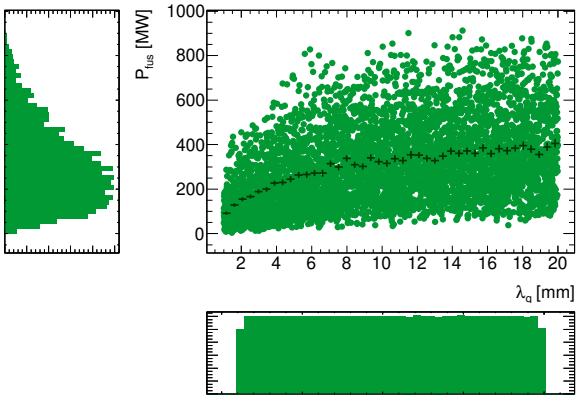

(b) P_{fus} projected on λ_q

Figure 2: λ_q Projection of the $L-H$ transition factor computed using the Martin scaling (left) and the fusion power (right). All the input of the ITER sensitivity study (B_T, f_H, $f_{n_{sep}}$, P_{NBI}, λ_q and S_q) has been varied using the ranged detailed in section 3.

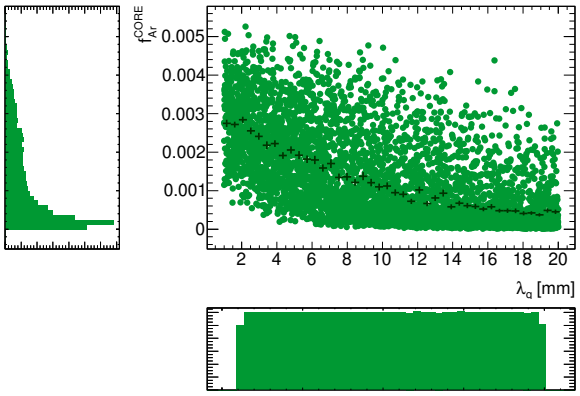

(a) f_{Ar}^{core} projected on λ_q

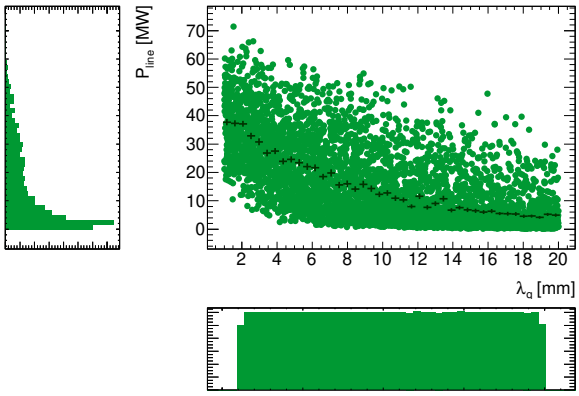

(b) P_{line} projected on λ_q

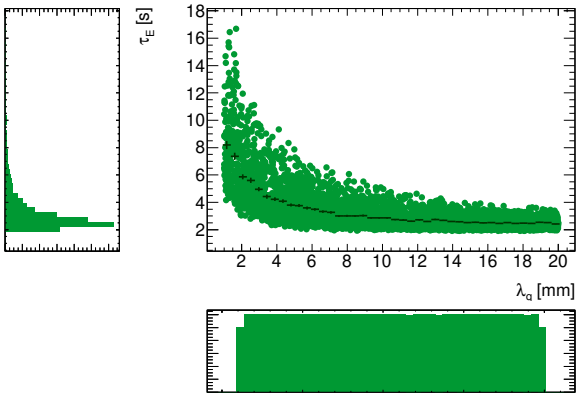

(c) τ_E projected on λ_q

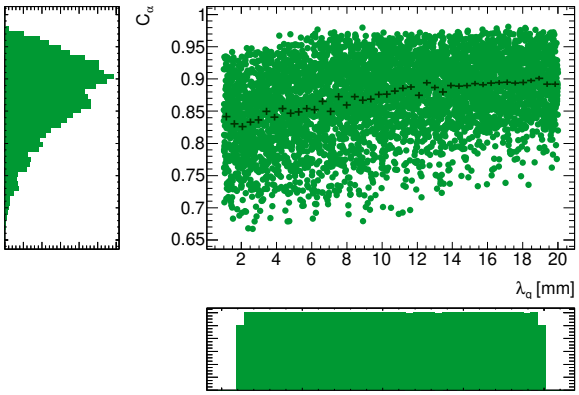

(d) C_α projected on λ_q

Figure 3: f_{Ar}^{core} (top left), P_{line} (top right), τ_E (bottom left) and C_α (bottom right) obtained with the *LHS* sampling described in 3.2.1, projected on λ_q.

the average P_{sep} value ($\sim$ 30). The lower the λ_q, the more the plasma cooling is driven by the argon effects, explaining the increased sensitivity of the plasma performances to f_{Ar}^{core} (*i.e.* to λ_q). Figure 3d shows the fusion reaction dilution factor C_α projected on λ_q. A larger dependency of the dilution effects is observed at lower λ_q, where the argon contribution is larger than the Helium one. This effects amplify the dependency to λ_q at low values. These two regimes are taken into account splitting the sensitivity analysis in two λ_q ranges : $[1-5]$ mm and $\lambda_q\,[5-20]$ mm.

3.2.2. Linear regression results

Figures 4 and 5 shows the f_{L-H} and P_{fus} standard regression coefficients, respectively. These rankings has been evaluated in the $\lambda_q\,[1-5]$ mm (left plots) and $\lambda_q\,[5-20]$ mm (right plots) ranges. Both linear (SRC, dark blue) and monotonous ($SRRC$, light blue) standard regressions coefficient are shown with their 95% confidences intervals (statistical uncertainties) and the variable R_{adj}, reflecting the quality of the linear fit, is precised. As $R_{adj} > 0.8$ for all the linear regression, their associated rankings are valid. A common feature of all rankings is the negligible S_q contribution. This result is coherent since the divertor constraint is driven by the plasma temperature at the divertor targets (in the baseline scenario $q_{peak} = 1.8\ \mathrm{MW\cdot m^{-2}}$ for $T_{target} = 5$ eV) and S_q does not affects T_{target} in the two points model.

Figure 4a shows that f_{L-H} is almost entirely driven by divertor constrains in the low λ_q regime, with comparable contribution from separatrix density ($SRC(f_{n_{sep}}) = 0.547$) and SOL width ($SRC(\lambda_q) = 0.348$). Figure 4b shows that $f_{n_{sep}}$ remains dominant in $\lambda_q \in [5-20]$ mm, while the λ_q sensitivity rank is twice smaller than in $\lambda_q \in [1-5]$ mm. The f_H and P_{add} contributions become comparable to the λ_q one, explaining the variance increase with λ_q suggested by figure 2 from section 3.2.1. Almost no contribution from the magnetic field is observed since the plasma performance improvement induced by a B_T increase is counterbalanced by the H-mode threshold increase.

The P_{fus} sensitivity rankings, shown in figure 5, indicate that the uncertainty associated to the additional power necessary to maintain the steady-state regime is largely dominated by the other inputs. This is explained by the need of larger argon impurity fraction to protect the divertor, that rises in average from 0.07% at for $P_{add} = 33$ MW to 0.2% for $P_{add} = 73$ MW. As a consequence, the average line radiation increases in average from 9 MW to 22 MW between $P_{add} = 33$ MW and $P_{add} = 73$ MW, while the $D-T$ fusion dilution factor decreases form 0.89 to 0.85. These two effects counterbalance the gain in performances induced by larger heating power, explaining the marginal P_{fus} sensitivity to P_{add} in the steady-state regime. The divertor constrains have a much stronger contribution at low λ_q (figure 5a) than at large λ_q (figure 5b) with $SRC(f_{n_{sep}}) = 0.273^{0.280}_{0.254}$ in $\lambda_q \in [1-5]$ mm and $SRC(f_{n_{sep}}) = 0.072^{0.082}_{0.064}$ in $\lambda_q \in [5-20]$ mm. The magnetic field (B_T) and the confinement (f_H) contributions are largely dominant for both ranges. The large B_T contribution is expected as the plasma current (I_p) is inversely proportional to B_T for a fixed q_{95} value and as I_p strongly drives the energy confinement ($\tau_E \propto I_p^{0.96}$) and the plasma density limit ($n_{GW} \propto I_p$).

3.2.3. Sobol method results

Some of the linear regression validity coefficients R_{adj} are close to 0.8, suggesting some non-linearities in the f_{L-H} and P_{fus} models. In this context, it is interesting to compare the $SRC/SRRC$ coefficients with Sobol indexes, computed without linearity assumptions. The comparison between first and total order Sobol indexes of each input also provides a quantification of its interactions with the other inputs. Finally, the first order Sobol indexes allow to test the additivity of the models, as their sum should be 1 for an additive model.

Figure 6 shows the first (S_{first}, dark blue) and the total (S_{total}, light blue) Sobol indexes evaluated for the f_{L-H} (top) and P_{fus} (bottom) figures of merits, in the $\lambda_q\,[1-5]$ mm (left) and $\lambda_q\,[5-20]$ mm (right) ranges. The first conclusion is that $SRC/SRRC$ and the first order Sobol indexes are equivalent (within the statistical uncertainties), validating the results shown in section 3.2.2. Even if twice more runs where used for this analysis, larger statistical uncertainties are observed for the Sobol indexes, highlighting the high statistical need of this method. The S_{total} indexes are generally larger than the S_{first} ones, indicating input interactions in the calculation of f_{L-H} and P_{fus}. The inputs that show the largest interactions for f_{L-H} are $f_{n_{sep}}$ and f_H. In the calculation of P_{fus}, the variables interactions are shared between the four dominants variables ($f_{n_{sep}}$, f_H, λ_q and B_T).

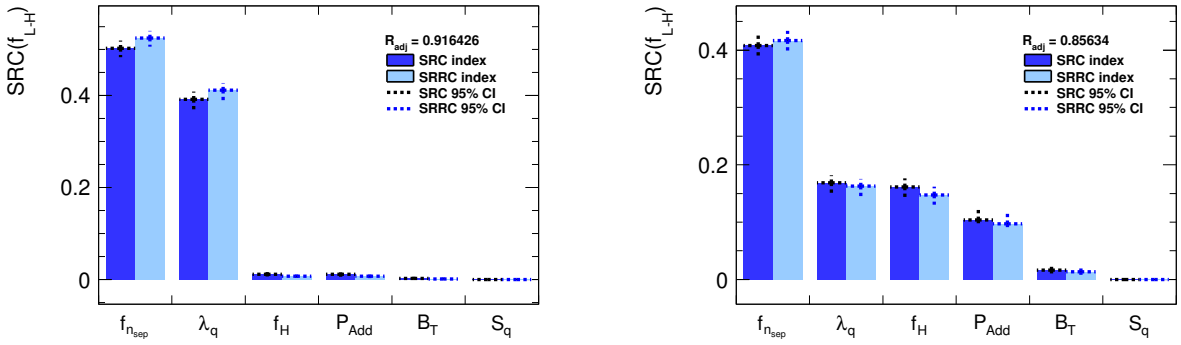

(a) $\lambda_q \in [1-5]$ mm (b) $\lambda_q \in [5-20]$ mm

Figure 4: Sensitivity indexes obtained from a linear (SRC, dark bule) and monotonic (SRRC, light blue) regression of f_{L-H} on the inputs considered in the ITER study, using the variation ranges described in section 3. The left and the right plots corresponds to the $\lambda_q\,[1-5]$ mm and $\lambda_q\,[5-20]$ mm ranges, respectively. The vertical error bars correspond to the 95% Confidence Intervals (CI) estimated using a Fisher Z-transform. The R_{adj} coefficient, describing the validity level of the linear hypothesis for the model is also precised (result invalidated for $R_{adj} < 0.8$).

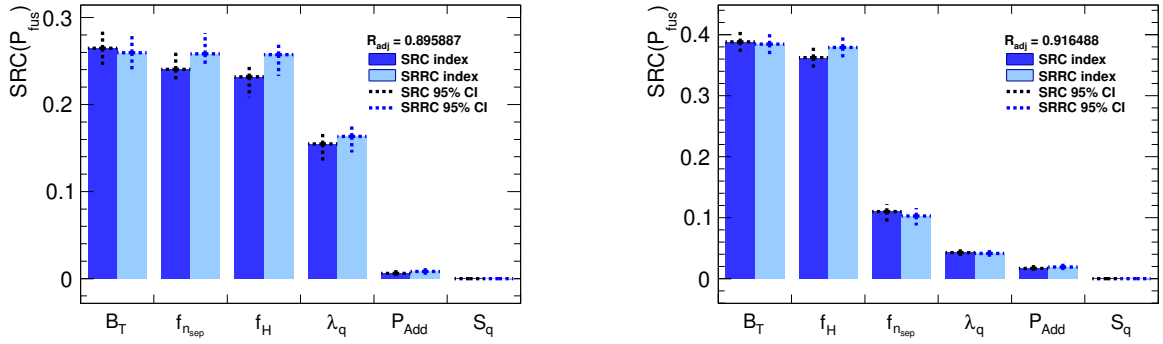

(a) $\lambda_q \in [1-5]$ mm (b) $\lambda_q \in [5-20]$ mm

Figure 5: Sensitivity indexes obtained from a linear (SRC, dark bule) and monotonic (SRRC, light blue) regression of P_{fus} on the inputs considered in the ITER study, using the variation ranges described in section 3. The left and the right plots corresponds to the $\lambda_q\,[1-5]$ mm and $\lambda_q\,[5-20]$ mm ranges, respectively. The vertical error bars correspond to the 95% Confidence Intervals (CI) estimated using a Fisher Z-transform. The R_{adj} coefficient, describing the validity level of the linear hypothesis for the model is also precised (result invalidated for $R_{adj} < 0.8$).

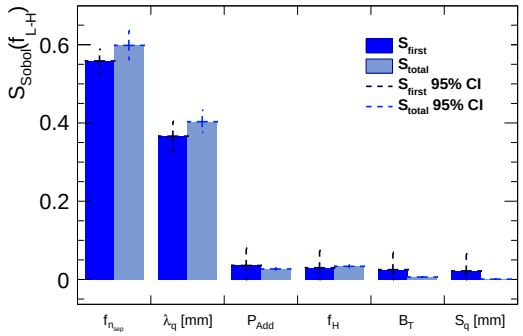

(a) $\lambda_q \in [1-5]$ mm

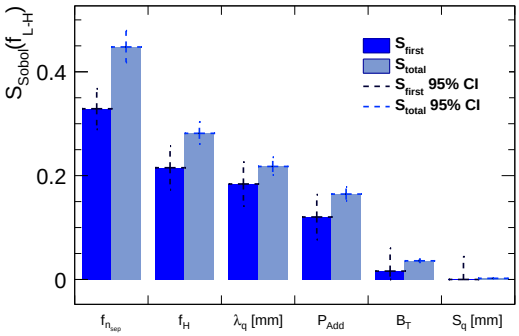

(b) $\lambda_q \in [5-20]$ mm

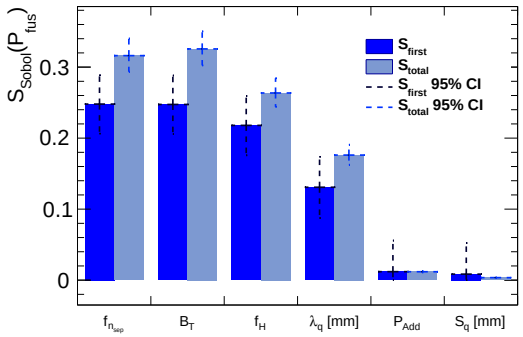

(c) $\lambda_q \in [1-5]$ mm

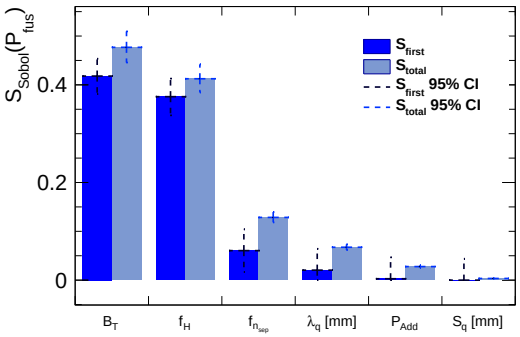

(d) $\lambda_q \in [5-20]$ mm

Figure 6: First (S_{first}, dark blue) and total (S_{total}, light blue) order Sobol indexes for the f_{L-H} (top) and P_{fus} (bottom) figures of merit, in the $\lambda_q\,[1-5]$ mm (left) and $\lambda_q\,[5-20]$ mm (right) ranges. The variation ranges of the other considered inputs are detailed in section 3. The vertical error bars correspond to the 95% Confidence Intervals (CI) estimated using a Fisher Z-transform.

4. DEMO 1 study

The second sensitivity analysis focuses on the European DEMO 2015 [14] pulsed design. The SYCOMORE inputs used to reproduce it are presented in table 2. To illustrate the potentiality of sensitivity analysis, all the main SYCOMORE inputs (48) are considered. As the uncertainties related to these parameters are not precisely known, a flat $\pm 10\%$ relative uncertainty is set for all inputs, except for R_{maj} which is kept constant for the reasons explained in 2.3. Parameters reflecting physical assumptions and engineering/scenario designs are considered in the same level. Such analysis allows to identify the variables that have the largest influence on the final design, driving the search for better tokamak modelling and technical improvements. Besides, if the model is linear, the rank of each input can be extrapolated to more realistic uncertainty ranges once they are estimated with dedicated analysis. Two effects must nevertheless be checked doing such extrapolation. Non-linear behaviour can appear for larger uncertainty ranges, invalidating the extrapolation. Secondly, if an input is strongly dominated by others, the output dependency may appear constant even if it has a non-linear behaviour. Reducing the uncertainty range of the dominant variables may reveal this non-linear behaviour, invalidating the extrapolation of the sensitivity indexes.

As the input phase-space is too large for a global linear regression or a Sobol sensitivity analysis, two steps are considered. First, Linear regressions are performed on sub-groups of 5 to 11 inputs related by their physical meaning, then the final Linear regression/Sobol analysis is performed on the dominant variables from each group. Although a Morris method could have been simply used, this strategy has been chosen for educational purpose as several sub-groups analysis illustrates different features of sensitivity methods. The chosen groups, presented in Appendix B are associated to the plasma shapes (5 variables), the plasma profiles (7 variables), the confinement (8 variables), the scrape-off layer (10 variables), the magnets systems (11 variables) and finally, the tritium breeding ratio, the vacuum vessel and the power balance variables (7 variables). The result of these analyses will be presented with a brief explanation of the physical cause of the ranking and discussion of statistical effects of interest if any. A global ranking will be then shown as a conclusion.

4.1. Sub-groups Results

4.1.1. Plasma shapes

A fair fraction of runs failure is observed (7.8%) on the sampling used to performed the plasma shape linear regression. As a linear regression can performed on any samplings, this method can be still applied in the presence of invalid designs (this is not the case of the Sobol and the Morris methods). This allows to evaluate the incidence of invalid design removal on sensitivity rankings. A bias can be induced either via input distribution alteration (through σ_{X_i}), either by the model dependency (through the linear regression coefficients β_i). In this situation, data visualization is necessary to understand and estimate the bias on the

Input definitions	**Names**	**DEMO 2015**
Major/minor plasma radius	R_{maj}/a_{min}	9.072/2.927 m
Toroidal magnetic field on plasma axis	B_T	5.667 T
Safety factor at 95% flux surface	q_{95}	3.247
Upper/lower separatrix elongation	κ^{up}/κ^{low}	1.672/1.983
Upper/lower separatrix triangularity	δ^{up}/σ^{low}	0.451/0.549
Greenwald electron density fraction	f_{GW}	1.20
IPB98(y,2) confinement enhancement factor	f_H	1.10
Additional heating power (NBI only)	P_{add}	50.0 MW
Heat flux on divertor targets	q_{peak}^{div}	<10 MW·m^{-2}
Plasma electron temperature on divertor	T_e^{div}	<5 eV
Argon screening	$\eta_{Ar} = \frac{f_{Ar}^{SOL}}{f_{Ar}^{CORE}}$	5.0
Upstream Scrape-off layer (SOL) width	λ_q/S_q	5.0/1.5 mm
Central/pedestal/separatrix density	$n_e^{0/ped/sep}$	1.01/0.77/0.45 $\cdot 10^{20}$m^{-3}
Central/pedestal/separatrix temperature	$T_e^{0/ped/sep}$	28/2.9/0.20 keV
Helium/argon fraction	f_{He}/f_{Ar}	7.91/0.65 %

Table 2: Main Inputs parameters used to define the DEMO 2015 working point. The parameters in the three last rows are computed by the SYCOMORE system code.

sensitivity ranking if possible.

Figure 7a, shows the 2D projection of the run convergence status over a_{min} and the upper plasma separatrix elongation (κ^{up}). Full green points corresponds to convergent runs and the empty gray diamonds to run failure caused by a too large tritium breeding blankets (BB) thickness (the BB neutronics code is only defined for a given BB thickness in SYCOMORE [5]). The lateral histograms show the a_{min} (bottom) and the κ^{up} (left) projection, the green and the gray part corresponds to valid design and to design with invalid BB, respectively. A non-valid input phase-space is observed at low a_{min}. In one hand, the bottom histogram from figure 7a shows that the a_{min} values of the failed designs are mostly far from the central value, decreasing $\sigma_{a_{min}}$ and thus $SRC(a_{min})$. On the other hand, the left histogram from figure 7a shows that the κ^{up} values of the failed designs are mostly close from the central value, increasing $\sigma_{\kappa^{up}}$ and thus $SRC(\kappa^{up})$.

The right plot of figure 7b shows the projection of the $P_{elec,net}$ on a_{min} with the $P_{elec,net}$ (left) and the a_{min} (bottom) histograms. The $P_{elec,net}$ mean value computed in a_{min} homogeneous intervals (horizontal bars) and its statistical uncertainty (vertical bars) is also shown for convergent (dark green) and all runs, including the invalid ones (dark blue). These profiles allow a visual estimation of the a_{min} linear regression coefficients ($\beta_{a_{min}}$) with and without invalid designs. Invalid breeding blanket (BB) width will only affect the net electricity production through the BB energy multiplication factor (M_e). As M_e is only varying by $\sim$ 0.1%, only a marginal bias is introduced in the $P_{elec,net}$ model. This is coherent with the important similarities observed between the blue (invalid designs included) and the green (invalid designs excluded) profiles. Figure 8 shows the linear regression coefficients removing (figure 8b) and keeping (figure 8a) the invalid designs. The linear approximation used for both rankings is valid as R_{adj} is well above 0.8. As expected, keeping the invalid designs increases (decreases) the a_{min} (κ^{up}) SRC coefficients by 4.6% (-7.6%). This effect is much larger than the $\sim$ 0.1% energy multiplication variation and thus, almost entirely due to the input distributions shapes distortion.

The plasma shape variable rankings on $P_{elec,net}$ and Δt_{pulse} shown on figures 9a-9b remain qualitatively valid as the number of failed runs is not large enough to modify the ranks hierarchy. $P_{elec,net}$ is dominated by both a_{min} and $\kappa^{up/low}$, whereas Δt_{pulse} is fully driven by a_{min}. The $P_{elec,net}$ ranking is explained by the plasma volume and energy confinement time dependency with a_{min} and $\kappa^{up/low}$. The κ^{low} SRC value is larger than the κ^{up} one as its baseline value is larger (10% variation range represents a larger absolute variation range if the central value is larger, increasing the relative SRC value). The pulse duration is also dependent on the remaining space for the Central Solenoid (CS), the larger the CS is, the longer the pulse will be. a_{min} directly drives the CS width, explaining the dominance of $SRC(a_{min})$ for the pulse duration.

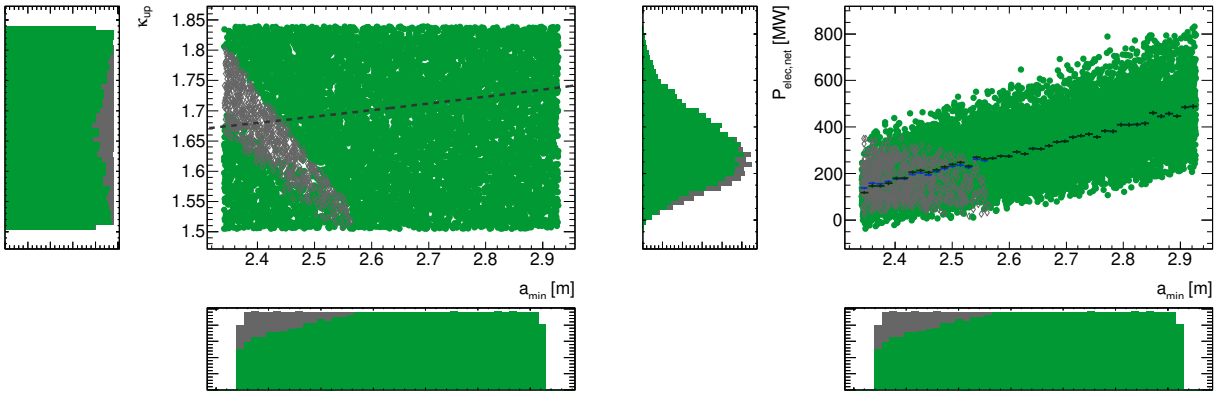

(a) (b)

Figure 7: Left : 2D projection of the convergence status over κ_{up} and a_{min} obtained with the sampling used for the plasma shape linear regression, with their corresponding 1D lateral histogram projections. The dotted grey line shows reasonability expected elongations as a function of a_{min} [35]. Right: $P_{elec,net}$ projection over a_{min} obtained with the same sampling, with their lateral histogram projections. The full green circles (empty gray diamonds) and the green (gray) histograms corresponds to valid (invalid breeding blanket BB geometry) designs. The dark green (blue) horizontal and vertical lines corresponds to the $P_{elec,net}$ mean values computed on regular bins and its statistical uncertainties computed removing (including) the invalid designs, respectively.

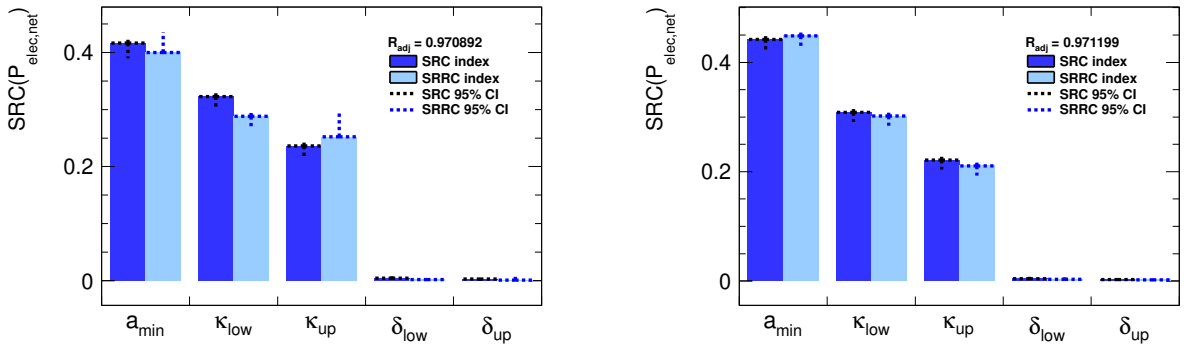

(a) Without invalid designs (b) With invalid designs

Figure 8: Linear (Blue, SRC) and monotonous (Light blue SRRC), standard regression coefficients on $P_{elec,net}$ computed on sample where invalid BB design has been removed (left) or kept (right). The errors bars corresponds to the statistical confidence level (CLs) computed using a Fisher Z-transform transform and the R_{adj} corresponds to the test of the model linearity, both described in section 2.2.1.

4.1.2. Plasma profiles

No invalid designs has been observed for the plasma profiles linear regressions and their linear test coefficient R_{adj} are well above 0.8 ($R_{adj} \in [0.93 - 0.98]$), validating their associated $SRC/SRRC$ rankings shown in figures 9c-9d. Figure 9c shows that $P_{elec,net}$ is largely dominated by f_{GW}, as a large average density value increases the fusion rate and helps the divertor protection (larger plasma separatrix density) simultaneously. A non-negligible influence from the pedestal top position (ρ_{ped}) on $P_{elec,net}$ is nevertheless observed. A $\pm 10\%$ variation of ρ_{ped} corresponds to a variation of the pedestal width of a factor 18 (from 1% to 18% of a_{min}). Such large variation mainly results from the parametrization of the code and do not corresponds to a realistic physical result.

Such effects are not present if the input uncertainty ranges are evaluated with realistic values, based on the current knowledge on plasma physics and engineering aspects as done in section 3. The temperature profile

parametrization implies that larger pedestal increases the central temperature for a given average temperature. Thanks to this effect the central temperature varies on average from 20 keV at $\rho_{ped} = 0.99$ to 37 keV at $\rho_{ped} = 0.81$. As a result, the fusion power varies from 1800 to 2050 MW, explaining the non-negligible ρ_{ped} sensitivity ranking. Finally, the $P_{elec,net}$ dependency on P_{add} appears to be negligible. A similar effect as the one discussed in section 3.2.2 is observed : larger heating power ($P_{add} \in [45 - 55]$ MW) increases the power flowing in the SOL, increasing the argon fraction used to protect the divertor ($f_{Ar} \in [0.625 - 0.650]$ %) and thus the fusion power through plasma cooling (line radiations ($P_{line} \in [163 - 168]$ MW) and fuel dilution ($C_\alpha \in [0.522 - 0.525]$). The heating power efficiency (30%) further reduces the beneficial effect of heating power on $P_{elec,net}$.

Figure 9d shows the result of the plasma shape variables linear regression on Δt_{pulse}. ρ_{ped} appears to be largely dominant with an almost negligible contribution from f_{GW}. Δt_{pulse} depends on plasma profiles through the bootstrap current fraction f_{BS}, the plasma ramp-up inductive flux consumption Φ_{ind} and the vertical flux Φ_{VF} production [2]. An increase of the pedestal width or f_{GW} will improve the burn duration through f_{BS} and Φ_{VF}, but will reduce it through Φ_{ind}. The results of the Δt_{pulse} sensitivity analysis show that this compensation effect limits the contribution from f_{GW} in a stronger way than for ρ_{ped}.

4.1.3. Confinement

Figures 9e and 9f show the plasma confinement inputs $SRC/SRCC$ rankings. No failed runs and R_{adj} >0.98 is observed, validating the linear regression results. The left plot shows that $P_{elec,net}$ is mainly driven by the safety factor at 95% flux surface (q_{95}). It is expected as q_{95} is inversely proportional to I_p, driving both the average electron density and the energy confinement time in a coherent way.

Figure 9f shows the result of the Δt_{pulse} linear regression. A weaker q_{95} dependency is observed, making the confinement enhancement factor f_H (and T_i/T_e in a lesser way) dominant. This result is expected since the f_H and T_i/T_e positive impact on Δt_{pulse} is not counterbalanced by a I_p value increase. As it is the case for q_{95}, larger I_p increases the need in CS flux for both ramp-up and flat-top. The $P_{elec,net}$ and Δt_{pulse} rankings both show a negligible argon screening $\eta_{Ar} = \frac{f_{Ar}^{SOL}}{f_{Ar}^{core}}$ dependency. This is confirmed by the apparent flat f_{Ar}^{core} dependency with η_{Ar} (within the statistical uncertainties). Two effects potentially explains this behavior : 70% of the line radiation is emitted from the core plasma, it is thus more efficient to increase f_{Ar}^{core} than increasing f_{Ar}^{SOL} to protect the divertor. Secondly, smaller f_{Ar}^{core} improves the fusion power. In this situation, larger power must be radiated with argon to protect the divertor targets, increasing the core and SOL average f_{Ar}. This effect dumps the f_{Ar}^{core} reduction obtained with larger argon screening. This effect is confirmed by the increase of the average f_{Ar}^{SOL} from 2.9% at $\eta_{Ar} = 4.5$ to 3.5% at $\eta_{Ar} = 5.5$ observed in the sampling used for the linear regression.

4.1.4. Scrape-off layer

Figures 9a and 9b show the SOL variables $SRC/SRRC$ ranks on $P_{elec,net}$ and Δt_{pulse}, respectively. In the DEMO baseline design, a relatively large λ_q is used (5 mm). The divertor constrains appears to be only driven by the target plasma temperature (T_{target}), with a divertor target energy flux $q_{peak} = 2.73$ MW$\cdot$m^{-2} well below the 5 MW$\cdot$m^{-2} limit for $T_{target} = 5$ eV. Thus, the only variables that are expected to have an impact on the design are λ_q, $f_{n_{sep}}$ and T_{target}^{max}, as the rest of the SOL inputs parametrizes the SOL power fluxes. $f_{n_{sep}}$ appears to be dominant for both $P_{elec,net}$ and Δt_{pulse} and λ_q sub-dominant with a 3-4 time lesser contribution. T_{target}^{max} appears to have a lesser impact.

4.1.5. Magnets

Figures 10a and 10b show the result of the $P_{elec,net}$ and Δt_{pulse} linear regressions on Central Solenoidal (CS) and Toroidal Field (TF) magnets parameters described in [6], respectively. $P_{elec,net}$ appears to be entirely driven by the toroidal magnetic field on plasma axis (B_T). This is expected as the rest of the variables only impact the electricity output though the radial build and magnets design validity parameters. As these effects are only captured through design validity criteria in SYCOMORE, such conventional sensitivity analysis brings no further understanding of the impact of the technical TF/CS characteristics on the net electricity production. Nevertheless, the impact of these parameters on the design can still be roughly evaluated using the Pareto front obtained with the SYCOMORE optimizer mode [8]. Figure 10b shows that B_T remains largely dominant for Δt_{pulse} with a small contribution of the CS/TF steel stress limit. More resistant steel structures reduces the necessary space by the magnets for a given flux/magnetic field production, leaving space for larger CS supraconductor quantity, resulting in Δt_{pulse} increase.

4.1.6. Breeding blankets (BB), vacuum vessel (VV) and power conversion group

Sensible tritium breeding ratio (TBR) values for a reactor design lies between 1.07 and 1.10. Hence a 10% variation around the baseline value (1.10) will be out of

the scope the SYCOMORE breeding blanket module was design for. Due to the way the BB module is coupled with SYCOMORE, this validity range triggers invalid designs for TBR > 1.10 and a flat BB thickness dependency with TBR for TBR < 1.07. In order to avoid dealing with invalid design, only a downward variation of the TBR has been considered. The TBR range of variation has not been reduced to keep a consistent relative range of variation with the other inputs, but also as it provides a clear and pedagogical example of a non-linear model, where only the Sobol method is valid.

Figures 10c and 10d show the result of the $P_{elec,net}$ and Δt_{pulse} linear regressions on the BB, VV and power conversion parameters. Figure 10c shows that $P_{elec,net}$ is only driven by the NBI wall plug efficiency since the auxiliary power fraction (f^{Aux}_{Power}) has a marginal effect and as other variables only affect $P_{elec,net}$ through design validity constrains. On the other hand, the Δt_{pulse} linear regression coefficients, shown in figure 10d are invalid as their associated $R_{adj} = 0.56$ is well below 0.8.

Figure 11 shows the projection of Δt_{pulse} over the target TBR prescribed by the user (TBR^{target}). As expected, two regimes are clearly identified: a flat Δt_{pulse} TBR^{target} dependency for $TBR^{target} < 1.07$ and a strong TBR^{target} dependency for $TBR^{target} > 1.07$. The flat regime is explained by the minimal BB thickness range of the BB module: if the BB width is below it minimal value, the minimal BB thickness is assumed in the design with TBR $= 1.07$, removing the radial build TBR^{target} dependency. In the $1.07 < TBR^{target} < 1.1$ range, the effect of TBR^{target} on the radial build, and hence on the CS coil thickness and the pulse duration, is captured as the BB module is well defined for this range of variation.

To obtain a well-defined Δt_{pulse} sensitivity ranking, the Sobol method is necessary. This method also indicates if the non-linearity arises only from the 1D Δt_{pulse} dependency (additive model) or from input interactions. Figure 12 shows the $SRC/SRRC$ (figure 12a) and the Sobol (figure 12b) Δt_{pulse} sensitivity of the BB, VV and power conversion inputs. In one hand, large differences are observed between the two TBR^{target} sensitivity indexes with $SRC(TBR^{target}) = 0.18$ for the linear regression and $S_{first} = 0.55$ for the Sobol method. Such differences are expected as the linear fit is largely dominated by the $TBR^{target} < 1.07$ range, representing 86% of the TBR^{target} input range. Thus the points from the $TBR^{target} > 1.07$ range will be ignored by the linear fit procedure as they have a negligible statistical weight resulting in a small linear coefficient and thus a sensitivity index underestimate. In the other hand, the two VV width (ΔR^{in}_{VV}) sensitivity indexes are quite close with $SRC(\Delta R^{in}_{VV}) = 0.4$ and $S_{first}(\Delta R^{in}_{VV}) = 0.43$. The sum of the Sobol index are close to 1 and the first and the total Sobol indexes are identical within the statistical uncertainties. Besides These two observations mean that the Δt_{pulse} model is additive with respect to TBR^{target} and ΔR^{in}_{VV}. As no interaction between TBR^{target} and ΔR^{in}_{VV} are observed, the linear regression can provide both a wrong estimate of the ranking (TBR^{target}) and a good one (ΔR^{in}_{VV}). As the model is additive, one would expect the SRC and the SRRC coefficients to be equal, which is not the case. This unexpected behavior arises from the flat dependency of Δt_{pulse} with TBR^{target} that breaks the monotonicity hypothesis assumed for $SRRC$ calculation, making the $SRRC$ coefficients evaluation ill-defined.

Another strategy to deal with the artificial non-linear Δt_{pulse} dependency with TBR^{target} would be reduce the TBR^{target} range of variation to [1.07, 1.10] and multiply its SRC coefficient by the ratio of the 10% variation and the [1.07, 1.10] one. Such extrapolation would assume a linear Δt_{pulse} dependency with TBR^{target} on the full 10% variation range. Hence, the results of this alternative method would have to be taken with grains of salt.

4.2. Final analysis

4.2.1. Input selection

The SRC ranks and the outputs RMS obtained in the previous sub-group analysis are used to select the inputs for the final sensitivity analysis. If this product of these two quantities is larger than 5%, the associated variable is retained. In decreasing order of importance, the selected inputs are $\{q_{95}, B_T, f_{GW}, a_{min}, \kappa_{low}, \kappa_{up}\}$ and $\{a_{min}, B_T, \rho_{ped}, f_H\}$ for $P_{elec,net}$ and Δt_{pulse}, respectively. Only two variables (a_{min}, B_T) are common in the initial final selections. a_{min} and B_T input has a contradictory impact on both $P_{elec,net}$ (positive effect) and Δt_{pulse} (negative effect). If the pulse duration constraint is a strong limiting factor, larger a_{min} or B_T might not be the best way to achieve optimal DEMO design while other variables such as f_H gets more interesting through their beneficial influence of both Δt_{pulse} and $P_{elec,net}$. Such consideration is well captured by the SYCOMORE optimizer.

This selection method is blind to cross-groups input interactions. If a variable has an important effect through its interactions with other inputs, this selection method might miss an important effect on Δt_{pulse} or $P_{elec,net}$. To avoid such situation, the selection is extended using a global Morris analysis. Such method only uses a few points per inputs and hence, its quan-

titative results are not well defined. For example, two identical Morris analysis often provide different sensitivity rankings. On the other hand, it is a stable and efficient method to identify negligible inputs or verify the input selection from another method. As the Morris algorithm fails if any run is removed, any BB invalid designs has been avoided setting the target TBR value to an arbitrary low value. Even though the results are not performed using the same radial build as the baseline design, this analysis remains adapted for an input selection validation. Figures 13a and 13b show the result of these validation studies for $P_{elec,net}$ and Δt_{pulse}, respectively. Although the Morris method shows consistent results with the initial selection, the $\{\rho_{ped},\ f_{n_{sep}}\}$ and $\{\frac{T_i}{T_e},\ f_{n_{sep}},\ \lambda_q\}$ variables shows non negligible $< |EE| >$ values for $P_{elec,net}$ and Δt_{pulse}, respectively. These variables have been added for the final analysis.

4.2.2. Results discussion

Both a_{min} and κ^{up} are varied for the $P_{elec,net}$ analysis. Hence a similar BB design invalidity issue as the one discussed in section 4.1.1 is observed. As shown in section 4.1.1, the $P_{elec,net}$ ranking is mostly affected by the effect of invalid design suppression on input distributions and only a negligible bias will be induced if such designs are kept. For this reason, the invalid BB width designs are not excluded for the $P_{elec,net}$ sensitivity analysis. Figure 14a shows the result of a Linear regression on $P_{elec,net}$ using the final extended input selection. Before discussing the sensitivity rankings in details, a first remark can be made about the input selection: the added variables (ρ_{ped} and $f_{n_{sep}}$) shows the smallest SRC rankings. This validates the initial variable selection method using the products between the SRC indexes and the RMS from the sub-groups.

Among the different input classes, the plasma shape parameters appear to have the largest impact on net electricity production ($\sum_i^{shape} SRC(X_i) = 0.46$), while the core plasma inputs (confinement and plasma profile parameters) has also a non-negligible influence on net electricity production with $\sum_i^{core\ pl} SRC(X_i) = 0.26$. The magnet system, has also an important influence with $SRC(B_T) = 0.21$. On the other hand, the SOL physics inputs influence on steady-state electricity production are fond to be almost negligible with $SRC(B_T) = 0.003$. This result may seem contradictory with the important sensitivity to SOL constrains shown in section 3 (ITER). It can be nevertheless explained by the 5 and 19 times smaller uncertainty range used for $f_{n_{sep}}$ and λ_q, respectively in the DEMO study. Moreover the DEMO working point is defined for $\lambda_q = 5$ mm and $f_{n_{sep}} = 0.6$, which is not in the range where the design is heavily dependent to the SOL constraints. On the other hand, the B_T uncertainty range is similar for the ITER and the DEMO study, explaining the much larger B_T sensitivity for similar figures of merit (P_{fus} and $P_{elec,net}$). Considering individual input rank, a_{min} and B_T appears to have the largest (positive) influence on $P_{elec,net}$ with $SRC(a_{min}) = SRC(B_T) = 0.21$. The (negative) impact of q_{95} remains considerable with $SRC(q_{95}) = 0.17$. Thus the potentially necessary q_{95} increase for plasma disruptions avoidance [36], may have an important influence on net electricity production. f_{GW} has also a non-negligible contribution to $P_{elec,net}$ with $SRC(f_{GW}) = 0.045$ as both the core and the SOL constraints are positively influence by this parameter. On the other hand, f_H only improves the core confinement and its positive effect is counterbalanced by the need of larger impurity fractions to protect the divertor plates, explaining its absence from the final ranking.

Figure 14b shows the pulse duration final sensitivity ranking. As a_{min} is varied, BB invalid designs are also present for the Δt_{pulse} final sensitivity analysis (8.1 %). As a_{min} value of all the invalid designs is much lower that the mean a_{min} value, an important bias is expected if invalid designs are removed from the sensitivity analysis and therefore should be kept. Using an arbitrarily small target TBR to avoid invalid BB designs should also be avoided as the target TBR drives the BB thickness that influence the CS size and hence Δt_{pulse}. The best compromise is therefore to keep the invalid designs even though a (relatively small) bias is expected from the failed runs, as the BB thickness is under-estimated for invalid runs. To estimate the effect of such bias on the final ranking, the linear regression ranking using $TBR_{target} = 1.1$ has been compared to same one, using $TBR_{target} = 1.09$ containing a much lesser amount of invalid designs (0.014%). Both rankings agrees within the statistical uncertainties, showing that keeping BB invalid designs only introduces a marginal bias on Δt_{pulse}.

Figure 14b show the final Δt_{pulse} linear regression ranking. As for the $P_{elec,net}$ one, all the input added after the Morris analysis are dominated by the one initially selected, validating the initial selection. The dominant input is a_{min} with $SRC(a_{min}) = 0.45$. a_{min} influences both the space left to the CS coil (negative impact on Δt_{pulse}) and the necessary CS flux for the plasma current ramp-up and a flat top of a given duration through Ψ_{ind}^{RU} and f_{BS} (positive impact on Δt_{pulse}). As Δt_{pulse} decreases with a_{min}, the radial build effect of a_{min} is dominant. Through their effects on the bootstrap current fraction, f_H and ρ_{ped} have

also an important impact on the pulse duration, with a cumulative SRC rank of 0.37.

4.2.3. Comparison with other sensitivity analysis

A simpler, but similar study [14] has been performed using the $PROCESS$ system code [9, 10]. Although the same outputs are considered ($P_{elec,net}$ and Δt_{pulse}), several differences in both of the statistical method and the tokamak modelling are present. A reduced number of inputs has been *a priori* selected for the initial $PROCESS$ analysis, while all the main $SYCOMORE$ inputs has been considered in the analysis presented in section 4, making sure that no significant effects are missed. Moreover, the inputs variables are varied one at time and hence, interactions are not captured in such analysis. Table 3 from [14, p10] shows the results of the initial DEMO 2015 analysis using $PROCESS$. The first remark is that the sensitivity on both B_T and q_{95} are not evaluated although their associated rankings shown in Figure 13a are significant for $P_{elec,net}$. Another difference is the presence of the helium (c_{He}) and the tungsten (c_W) concentration in the inputs considered in the $PROCESS$ sensitivity analysis. These two variables are not present in $SYCOMORE$ as the Helium fraction is consistently calculated with the fusion rate, the energy confinement and the ratio between the Helium and the energy confinement and as tungsten impurity are not considered. For these reasons, only qualitative comparisons should be made between the two analysis.

The dominant input for $P_{elec,net}$ evaluated by the $PROCESS$ analysis appears to be the plasma elongation at the 95% flux surface (κ_{95}), driving twice larger differences that the aspect ratio (A). This result should be compared with the sum of upper and lower elongation SRC indexes, as a 10% variation of the upper/lower elongation only drives a 5% variation on the total one. Therefore, the two analysis qualitatively agree as Figure 14a shows that $SRC(\kappa_{low}) + SRC(\kappa_{up}) > SRC(a_{min})$. The sub-dominant parameter in the initial DEMO 2015 sensitivity analysis is A. As R_{maj} is also fixed for this analysis and A is only varied by 10% ($d(\frac{1}{a_{min}}) = -da_{min}$), such uncertainty source is equivalent to the a_{min} one. The A sensitivity is hence coherent with the large a_{min} SRC shown in Figure 13a. $P_{elec,net}$ is quite sensible to f_{GW} (referred as $\frac{<n_{li}>}{n_{GW}}$ in [14]) in both analyses. The main contradiction between the two analysis concerns f_H (referred as H in [14]): this paper shows that f_H has a negligible effect on $P_{elec,net}$ while [14, p10] shows a non-negligible sensitivity to this parameter. The $SYCOMORE$ result can be explained by the increase of the impurity fraction for divertor protection, inducing more line radiation and $D-T$ fuel dilution. The apparent contradictory $PROCESS$ result potentially results form the different choice of the radiative impurity (Argon for $SYCOMORE$ and Xenon for $PROCESS$), the absence of tungsten impurity in $SYCOMORE$ and the difference in the way Helium concentration is treated. In one hand the Xenon and tungsten induces less $D-T$ fuel dilution for a given radiated power, the effect of impurity seeding increase for divertor protection due to better confinement is lesser in the $PROCESS$ runs. On the other hand the Helium fraction is fixed in $PROCESS$, while the increase of f_{He} due to larger P_{fus} is captured in $SYCOMORE$. Both effects tend to reduce the f_H improvement effect on $P_{elec,net}$ in $SYCOMORE$ with respect to $PROCESS$. Nevertheless, this discussion has to be taken with grains of salts as many other difference are present in both the sensitivity analysis and the system codes models (for example $SYCOMORE$ use an advanced two points model while the SOL physics is only taken into account with a $\frac{P_{sep}}{R_{maj}}$ ratio in the $PROCESS$ DEMO 2015 analysis).

5. Conclusion

The SYCOMORE system code is a modular and coherent set of modules, simulating the major elements of a fusion reactor. New advanced sensitivity algorithms have been recently added allowing to identify the most important engineer/physical parameters for a given figure of merit. This helps the selection of parameters considered in optimization and uncertainty propagation. Sensitivity algorithms bring also precious information about the model (linearity, additivity, variables interactions with others etc...). This can be helpful as compensations effects are often observed in system codes leading to non-intuitive results. A full set of algorithms are implemented: Morris screening, linear/monotonous regression and Sobol method, allowing to get meaningful sensitivity rankings for most of the situations. Moreover the Linear/monotonous regression and the Sobol methods provide also confidence intervals reflecting the statistical uncertainty on the ranks. This is crucial to prevent from false ranking due to lack of statistics (number of input cases used for the evaluation).

Section 3 presents the test of the new sensitivity tools on the ITER design, using 6 input variables. The intervals used for the variation of the selected inputs have been chosen to reflect known uncertainties on the magnets and plasma performances. The sensitivity of the fusion power (P_{fus}) and of the $L-H$ threshold (f_{L-H}) with these inputs has been evaluated using data visualization, linear regression and the Sobol

method, providing a comprehensive illustration of the methods for the user. Two sensitivity regimes have been observed, depending on λ_q ($\lambda_q \in [1-5]$ mm and $\lambda_q \in [5-20]$ mm), with a dominant contribution of the SOL parameters for both P_{fus} and f_{L-H} in the low λ_q regime and dominant contribution of the confinement and toroidal field uncertainties at high λ_q. Stronger dependencies on the SOL parameters have also been observed for the H-mode threshold than for fusion power.

In section 4, a wider sensitivity analysis has been shown on the DEMO 2015 design using 48 variable inputs. A different strategy has been used for their variation range ($\pm 10\%$ around the baseline value) as not all the uncertainties are precisely known for these parameters. The sensitivity of the net electric power produced by the fusion power plant ($P_{elec,net}$) and the pulse duration (Δt_{pulse}) with the 48 inputs has been evaluated, considering first linear regressions on inputs sub-groups to select dominant variables, and then a final sensitivity analysis on dominant variables. The first step allowed to illustrate several features of the methods, such as the impact of invalid designs (section 4.1.1), the method behavior with a non-linear model (section 4.1.6) and the example where sensitivity analysis does not provide meaningful result (section 4.1.5).

The dominant variable selection is different for $P_{elec,net}$ and Δt_{pulse}. For example the plasma elongations has been selected for the $P_{elec,net}$ and not for Δt_{pulse}, while f_H is selected for Δt_{pulse} but not for $P_{elec,net}$. Plasma size and shaping appears to have major impact on $P_{elec,net}$ taking 50% of its sensitivity. The toroidal magnetic field has also a major impact on $P_{elec,net}$, taking 23% of his sensitivity. A strong impact of the security factor q_{95} has also been observed with 17%, showing that disruption avoidance using larger q_{95} has a great impact on the power plant performances. Surprisingly, a minor impact of the plasma confinement has been observed on $P_{elec,net}$ for this design while the Greenwald density fraction sensitivity is not negligible (4.5%). The pulse duration sensitivity is largely dominated by a_{min} through its impact on the remaining space for the CS coil, taking 45% of the sensitivity. On the other hand, plasma physics parametrization (f_H and ρ_{ped}) takes a non-negligible fraction of Δt_{pulse} sensitivity (37%). For the future, a similar DEMO study using realistic uncertainty range for the 48 inputs is foreseen. The implementation of advanced sensitivity algorithms evaluating the inputs sensitivity through their impact on design validity is also planned to complete the understanding provided by sensitivity analysis on fusion power plant designs.

6. Acknowledgments

This work has been carried out within the framework of the EUROfusion Consortium and has received funding from the Euratom research and training programme 2014-2018 and 2019-2020 under grant agreement No 633053. The views and opinions expressed herein do not necessarily reflect those of the European Commission.

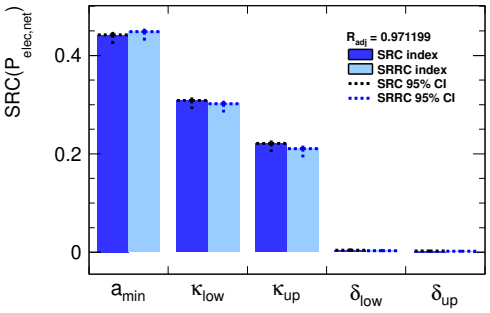

(a) Plasma shape

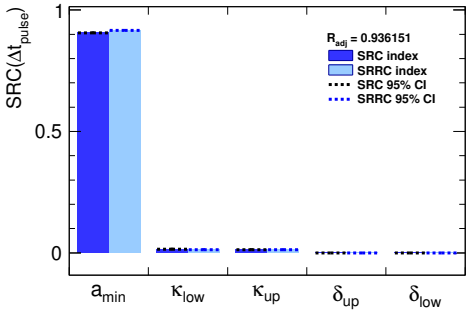

(b) Plasma shape

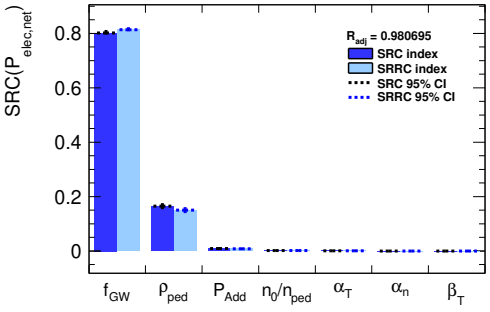

(c) Plasma profiles

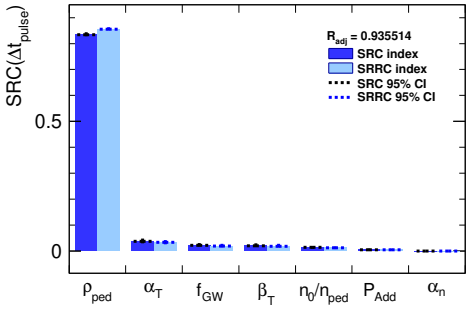

(d) Plasma profiles

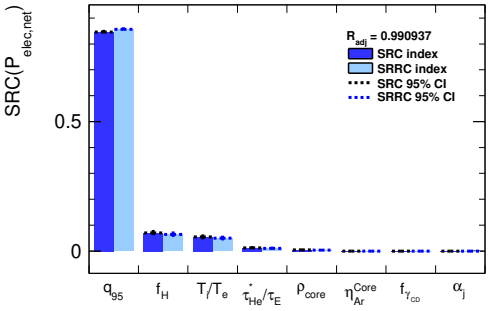

(e) Confinement

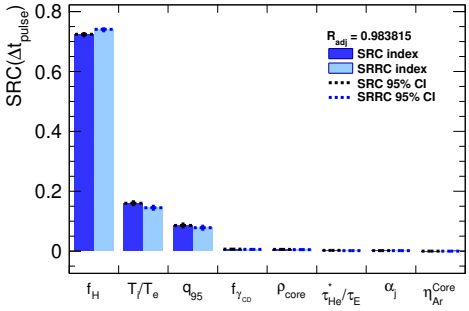

(f) Confinement

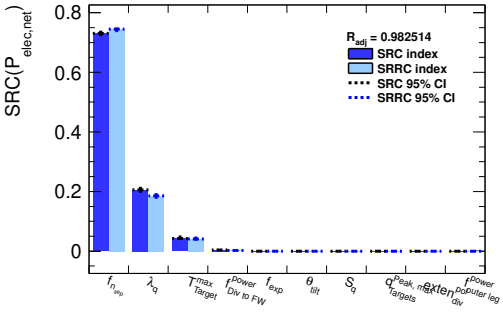

(g) Scrape-off layer

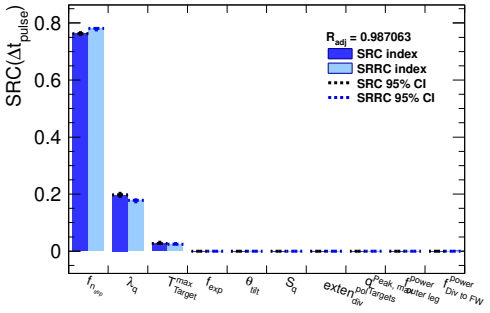

(h) Scrape-off layer

Figure 9: Linear (Blue, SRC) and monotonous (Light blue SRRC), standard regression coefficients on $P_{elec,net}$ (left) and Δt_{pulse} (right), computed using a LHS sampling of 1000 points per inputs variables. Each line corresponds to the different variables plasma physics sub-set described in section 4. The errors bars corresponds to the statistical confidence level (CLs) computed using a Fisher Z-transform transform and the R_{adj} corresponds to the test of the model linearity, both described in section 2.2.1.

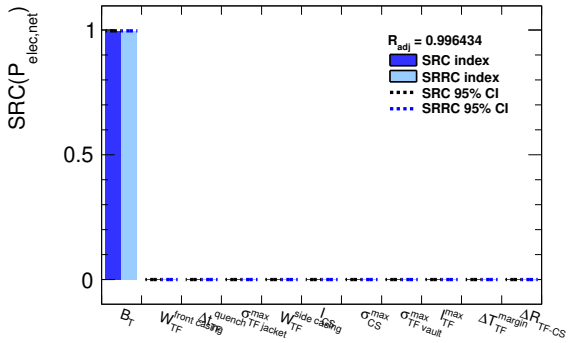

(a) Magnets parameters

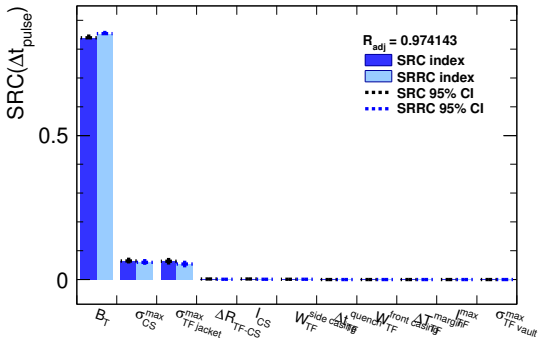

(b) Magnets parameters

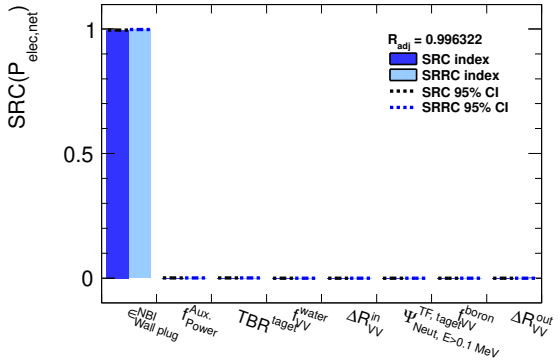

(c) Breeding blankets and power conversion

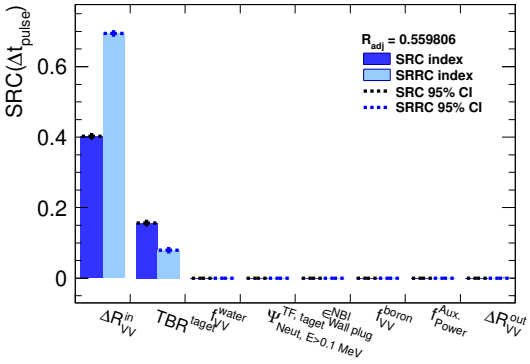

(d) Breeding blankets and power conversion

Figure 10: Linear (Blue, SRC) and monotonous (Light blue SRRC), standard regression coefficients on $P_{elec,net}$ (left) and Δt_{pulse} (right). Each line corresponds to the different engineering parameter input sub-set described in section 4. The errors bars corresponds to the statistical confidence level (CLs) computed using a Fisher Z-transform transform and the R_{adj} corresponds to the test of the model linearity, described in section 2.2.1.

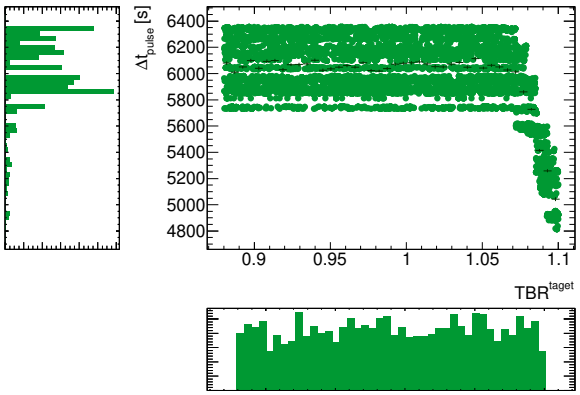

Figure 11: Projection of the Δt_{pulse} value on TBR^{target} obtained in the LHS sampling used in the BB, VV and power conversion group linear regression (green points). The mean value (horizontal dark green bars) computed on homogenous bins and it associated statistical uncertainty (vertical dark green bars) is added.

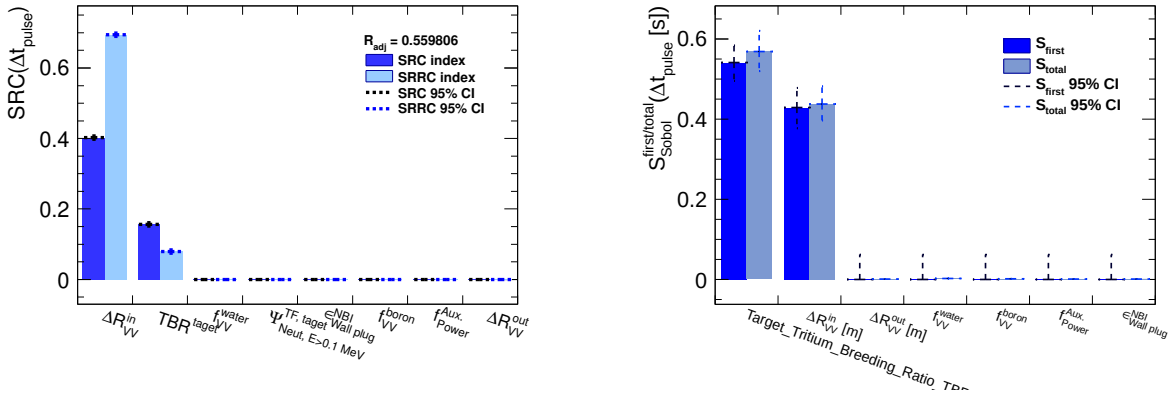

(a) Linear regression (b) Sobol indexes

Figure 12: Standard regression coefficients (left plot) and Sobol indexes (right plot) computed to evaluated the sensitivity of the pulse duration with respect to BB, VV and power conversion inputs parameters 10% variations. The dark blue indexes corresponds to SRC (left) and S_{first} (right) indexes and the light blue to $SRRC$ (left) and S_{total} indexes (right) (see section 2). The statistical 95% confidence intervals are deduced from Z-Fisher transformations.

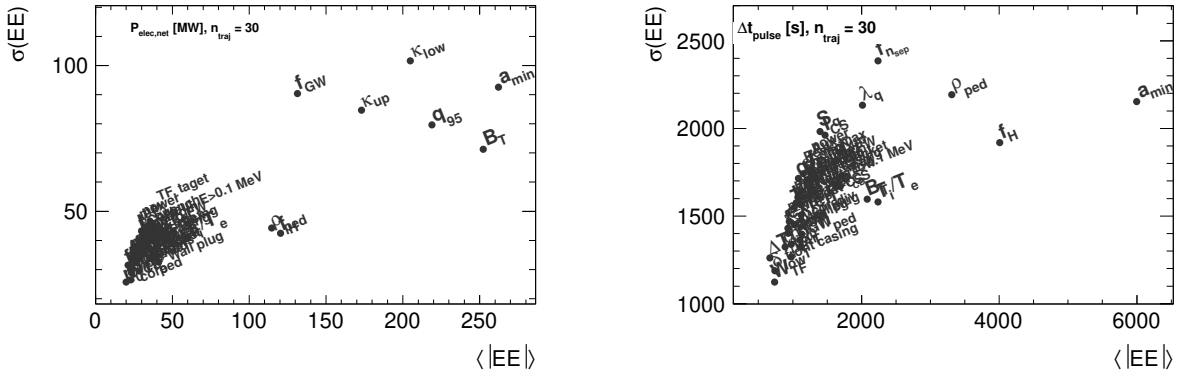

(a) $P_{elec,net}$ (b) Δt_{pulse}

Figure 13: RMS of the EE as a function of their mean absolute value calculated using the Morris screening method for all the 38 inputs considered in the DEMO 2015 study using 5 trajectories. An arbitrary low target TBR value has been used to avoid non-valid designs in this analysis.

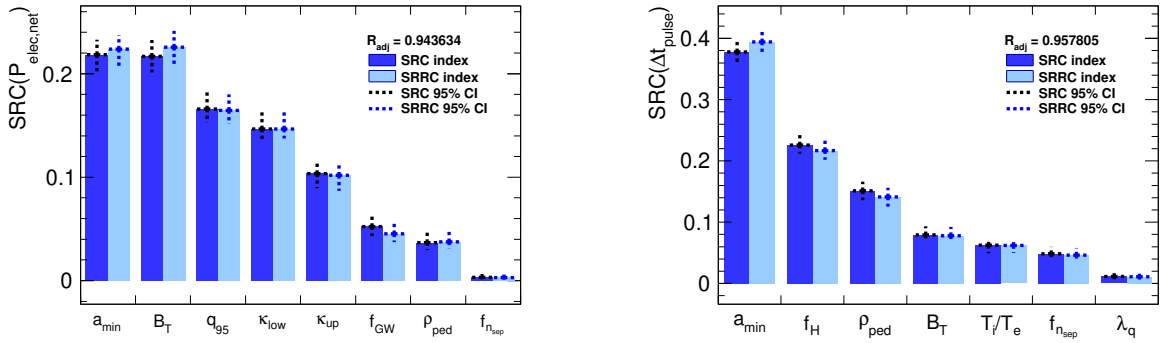

(a) (b)

Figure 14: Final Linear (Blue, SRC) and monotonous (Light blue SRRC), standard regression coefficients on $P_{elec,net}$ (left) and Δt_{pulse} (right) performed on dominant variables (selection described in section 4.2). The errors bars corresponds to the statistical confidence level (CLs) computed using a Fisher Z-transform transform and the R_{adj} corresponds to the test of the model linearity, both described in section 2.2.1.

Appendix A. Helios (core plasma) - Soldiv (SOL) loop

The Helios (core plasma) and the SOLDIV (SOL) codes are interfaced using three embedded loops:

(i) **Separatrix consistency loop**
The electronic separatrix temperature (T_e^{sep}) is both an input for Helios and an output from the two points model, depending on the separatrix power calculated by Helios. This loops ensure a consistent T_e^{sep} value by iteratively equalizing the Helios T_e^{sep} value with the one calculated by SOLDIV.

(ii) **Minimal impurity fraction**
Once consistent boundary condition is obtained, the minimal impurity fraction needed to protect from intolerable divertor heat loads and sputtering is calculated. This loops estimates the minimal impurity fraction necessary to ensure the two following conditions : $q_{peak}^{div} < q_{peak,max}^{div}$ (protection form heat loads) and $T_{Target} < T_{Target}^{max}$ (protection for tungsten sputtering).

(iii) **Density averaged temperature** $< T_e >_n$
$< T_e >_n$ was an input in the former version of SYCOMORE. In order to avoid inconsistent steady-state power balance leading to invalid designs and to make the input more, a new option has been set to use the additional power (P_{add}) as an input value instead of $< T_e >_n$. Technically this parametrization is implemented by adding an other loop that estimates the minimal $< T_e >_n$ value for which P_{add} matches with the prescribed value.

Appendix B. SYCOMORE variables definitions

Plasma shape		
Minor plasma radius	a_{min} [m]	Engineer
Lower separatrix elongation	κ^{low}	Engineer
Upper separatrix elongation	κ^{up}	Engineer
Lower separatrix triangularity	σ^{low}	Engineer
Upper separatrix triangularity	δ^{up}	Engineer
Plasma profiles		
Greenwald electron density fraction	f_{GW}	Engineer
Top pedestal normalized plasma radius	ρ_{ped}	physics
Additional heating power (NBI only for DEMO 2015)	P_{add} [MW]	Engineer
density profile peaking parameter	$\frac{n_e(0)}{n_e(ped)}$	physics
alpha density profiles parameter	α_n	physics
alpha temperature profiles parameter	α_T	physics
beta temperature profiles parameter	βT	physics
Confinement		
IPB98(y,2) confinement enhancement factor	f_H	physics
Safety factor at 95% flux surface	q_{95}	Engineer
Ratio between ions and electrons temperatures	$\frac{T_i}{T_e}$	physics
Ratio between effective He and energy confinement	$\frac{\tau_{He}}{\tau_E}$	Engineer
Core plasma normalized plasma radius	ρ_{core}	physics
Current drive efficiency coeficient	$f_{\gamma_{CD}}$	physics
Ratio between SOL and core argon fraction	$\eta_{Ar} = \frac{f_{Ar}^{SOL}}{f_{Ar}^{core}}$	physics
Current density peaking factor	α_j	physics
Scrape-off layer (SOL)		
Separatrix density parameter	$f_{n_{sep}} = \frac{n_e(sep)}{f_{GW} n_{GW}}$	Engineer/physics
Upstream SOL energy density width	λ_q [mm]	Physics
SOL private region spreading factor	S_q [mm]	Physics
SOL flux expansion	f_{exp}	Physics
Target tilt angle	θ_{tilt}	Engineer
Maximum plasma temperature on divertor targets	T_{Target}^{max} eV	Engineer
Maximum heat flux on divertor targets	$q_{Target}^{peak,max}$ [$\mathrm{MW \cdot m^{-2}}$]	Engineer
Fraction of power on outter divertor targets	f_{outer}^{power}	Physics
Fraction of power radiated from divertor to first wall	$f_{DivtoFW}^{power}$	Physics
Divertor poloidal extension	$exten_{div}^{pol}$	Engineer

Table B1: Description of the plasma physics variables used in the different groups defined in section 4. The third row specify if the input is a parametrization of the model assumptions (physics) or a parametrization of the scenario/power plant design (engineer).

Magnets		
Toroidal field on plasma axis	B_T [T]	Engineer
Maximum stress on TF coil jacket TF front casing thickness	$W_{TF}^{frontcasing}$ [m]	Engineer
TF side casing thickness	$W_{TF}^{sidecasing}$ [m]	Engineer
Maximum stress on TF coil jacket	$\sigma_{TFjacket}^{max}$ [Pa]	Engineer
Maximum stress on TF coil vault	$\sigma_{TFvault}^{max}$ [Pa]	Engineer
TF maximum current	I_{TF}^{max} [A]	Physics
TF quench detection delay	Δt_{TF}^{quench} [s]	Physics
TF temperature margins	$T_{TF}^{margins}$ [K]	Physics
Gap between TF and CS coils	ΔR_{TF-CS} [m]	Engineer
CS maximum stress	σ_{CS}^{max} [Pa]	Engineer
CS maximum current	I_{CS}^{max} [A]	Physics
Breeding blankets (BB), Vacuum vessel (VV) and power conversion		
Target tritium breeding ratio	TBR^{target}	Engineer
Maximum fast neutron flux on TF coil	$\Psi_{Neut,E>0.1}^{TF,targ}$ [$m^{-2}.s^{-1}$]	Engineer
Inner VV thickness	ΔR_{VV}^{in} [m]	Engineer
Outer VV thickness	ΔR_{VV}^{out} [m]	Engineer
VV Boron fraction	f_{VV}^{boron}	Engineer
VV water fraction	f_{VV}^{water}	Engineer
NBI wall plug efficiency	$\epsilon_{Wallplug}^{NBI}$	Engineer
Fraction of power used for auxiliary systems	f_{power}^{Aux}	Engineer

Table B2: Description of the variables used in the different groups magnets, breeding blanket, vacuum vessel and power conversion groups defined in section 4. The third row specify if the input is a parametrization of the model assumptions (physics) or a parametrization of the scenario/power plant design (engineer).

[1] Reux C, Gallo L D, Imbeaux F, Artaud J F, Bernardi P, Bucalossi J, Ciraolo G, Duchateau J L, Fausser C, Galassi D, Hertout P, Jaboulay J C, Li-Puma A, Saoutic B and and L Z 2015 *Nuclear Fusion* **55** 073011

[2] Johner J 2011 *Fusion Science and Technology* **59** 308–349

[3] Stangeby P C 2000 *The Plasma Boundary of Magnetic Fusion Devices* (IOP Publishing Ltd)

[4] Jaboulay J C, Puma A L and Arroyo J M 2013 *Fusion Engineering and Design* **88** 2336 – 2342 ISSN 0920-3796 proceedings of the 27th Symposium On Fusion Technology (SOFT-27); Lige, Belgium, September 24-28, 2012

[5] Li-Puma A, Jaboulay J C and Martin B 2014 *Fusion Engineering and Design* **89** 1195 – 1200 ISSN 0920-3796 proceedings of the 11th International Symposium on Fusion Nuclear Technology-11 (ISFNT-11) Barcelona, Spain, 15-20 September, 2013

[6] Zani L, Artaud J , Boutry A, Gallo L D, Duchateau J , Hertout P, Kahn S, Piot N, Reux C, Sad J and Torre A 2018 *IEEE Transactions on Plasma Science* **46** 3109–3114 ISSN 0093-3813

[7] Dardour S 2013 Development of an energy conversion module for the sycomore platform Tech. rep. CEA Nuclear Energy Division Internal report

[8] Reux C, Kahn S, Zani L, Pgouri B, Piot N, Owsiak M, Aiello G, Artaud J F, Boutry A, Dardour S, Gallo L D, Duchateau J L, Galassi D, Imbeaux F, Jaboulay J C, Magaud P, Said J, Saoutic B and Sardain P 2018 *Fusion Engineering and Design* **136** 1572 – 1576 ISSN 0920-3796 special Issue: Proceedings of the 13th International Symposium on Fusion Nuclear Technology (ISFNT-13)

[9] Kovari M, Kemp R, Lux H, Knight P, Morris J and Ward D 2014 *Fusion Engineering and Design* **89** 3054 – 3069 ISSN 0920-3796

[10] Kovari M, Fox F, Harrington C, Kembleton R, Knight P, Lux H and Morris J 2016 *Fusion Engineering and Design* **104** 9 – 20 ISSN 0920-3796

[11] Lux H, Kemp R, Wenninger R, Biel W, Federici G, Morris W and Zohm H 2017 *Fusion Engineering and Design* **123** 63 – 66 ISSN 0920-3796 proceedings of the 29th Symposium on Fusion Technology (SOFT-29) Prague, Czech Republic, September 5-9, 2016

[12] Shimada M, Campbell D, Mukhovatov V, Fujiwara M, Kirneva N, Lackner K, Nagami M, Pustovitov V, Uckan N, Wesley J, Asakura N, Costley A, Donné A, Doyle E, Fasoli A, Gormezano C, Gribov Y, Gruber O, Hender T, Houlberg W, Ide S, Kamada Y, Leonard A, Lipschultz B, Loarte A, Miyamoto K, Mukhovatov V, Osborne T, Polevoi A and Sips A 2007 *Nuclear Fusion* **47** S1–S17

[13] ITER Organization 2018 Iter research plan within the staged approach (level iii provisional version) Tech. Rep. ITR-18-003 ITER

[14] Wenninger R, Kembleton R, Bachmann C, Biel W, Bolzonella T, Ciattaglia S, Cismondi F, Coleman M, Donné A, Eich T, Fable E, Federici G, Franke T, Lux H, Maviglia F, Meszaros B, Ptterich T, Saarelma S, Snickers A, Villone F, Vincenzi P, Wolff D and Zohm H 2016 *Nuclear Fusion* **57** 016011

[15] Saltelli A, Tarantola S, Campolongo F and Ratto M 2004 *Sensitivity Analysis in Practice: A Guide to Assessing Scientific Models* (Wiley)

[16] Saltelli A, Tarantola S, Campolongo F, Ratto M, Andres T, Cariboni J, Gatelli D and Saisana M 2008 *Global Sensitivity Analysis: The Primer* (Wiley)

[17] Blanchard, Jean-Baptiste, Damblin, Guillaume, Martinez, Jean-Marc, Arnaud, Gilles and Gaudier, Fabrice 2019 *EPJ Nuclear Sci. Technol.* **5** 4 URL `https://doi.org/10.1051/epjn/2018050`

[18] Iman R, Shortencarier M and Johnson J 1985 *Sandia National Laboratories*

[19] Morris M D and Mitchell T J 1995 *Journal of Statistical Planning and Inference* **43** 381 – 402 ISSN 0378-3758

[20] Homma T and Saltelli A 1996 *Reliability Engineering and System Safety* **52** 1 – 17 ISSN 0951-8320

[21] Martinez J 2011 Analyse de sensibilit globale par dcomposition de la variance Tech. rep. institut Henri Poincare

[22] McKay M D, Beckman R J and Conover W J 2000 *Technometrics* **42** 55–61

[23] Fisher R A 1921 *Metron* **1** 3–32

[24] Owen A B 2014 *SIAM/ASA Journal on Uncertainty Quantification* **2** 245–251

[25] Li H S 2013 *Journal of Mechanical Science and Technology* **27** 1021–1029 ISSN 1976-3824 URL `https://doi.org/10.1007/s12206-013-0227-3`

[26] Challis C, Garcia J, Beurskens M, Buratti P, Delabie E, Drewelow P, Frassinetti L, Giroud C, Hawkes N, Hobirk J, Joffrin E, Keeling D, King D, Maggi C, Mailloux J, Marchetto C, McDonald D, Nunes I, Pucella G, Saarelma S and and J S 2015 *Nuclear Fusion* **55** 053031

[27] Kukushkin A, Pacher H, Loarte A, Komarov V, Kotov V, Merola M, Pacher G and Reiter D 2009 *Nuclear Fusion* **49** 075008

[28] Artaud J, Imbeaux F, Garcia J, Giruzzi G, Aniel T, Basiuk V, Bécoulet A, Bourdelle C, Buravand Y, Decker J, Dumont R, Eriksson L, Garbet X, Guirlet R, Hoang G, Huynh P, Joffrin E, Litaudon X, Maget P, Moreau D, Nouailletas R, Pégourié B, Peysson Y, Schneider M and Urban J 2018 *Nuclear Fusion* **58** 105001

[29] Eich T, Leonard A, Pitts R, Fundamenski W, Goldston R, Gray T, Herrmann A, Kirk A, Kallenbach A, Kardaun O, Kukushkin A, LaBombard B, Maingi R, Makowski M, Scarabosio A, Sieglin B, Terry J, Thornton A and and 2013 *Nuclear Fusion* **53** 093031

[30] ITER Physics Expert Group on Divertor and ITER Physics Expert Group on Divertor Database and ITER Physics Basis Editors 1999 *Nuclear Fusion* **39** 2391–2469

[31] Eich T, Sieglin B, Scarabosio A, Fundamenski W, Goldston R J and Herrmann A (ASDEX Upgrade Team) 2011 *Phys. Rev. Lett.* **107**(21) 215001

[32] ITER Physics Expert Group on Confin Transport and ITER Physics Expert Group on Confin Database and ITER Physics Basis Editors 1999 *Nuclear Fusion* **39** 2175–2249

[33] Martin Y R, Takizuka T and the ITPA CDBM H-mode Threshold Data Group 2008 *Journal of Physics: Conference Series* **123** 012033

[34] Chang C, Ku S, Loarte A, Parail V, Kchl F, Romanelli M, Maingi R, Ahn J W, Gray T, Hughes J, LaBombard B, Leonard T, Makowski M and Terry J 2017 *Nuclear Fusion* **57** 116023

[35] Zohm H, Angioni C, Fable E, Federici G, Gantenbein G, Hartmann T, Lackner K, Poli E, Porte L, Sauter O, Tardini G, Ward D and Wischmeier M 2013 *Nuclear Fusion* **53** 073019

[36] PC de Vries MF Johnson I S and JET EFDA Contributors 2009 *Nuclear Fusion* **49** 055011